Hindawi
Advances in Materials Science and Engineering
Volume 2021, Article ID 5539854, 23 pages
https://doi.org/10.1155/2021/5539854

Research Article

Effect of Glutinous Rice Slurry on the Reinforcement of Silt in the Yellow River Basin by Microbially Induced Carbonate Precipitation (MICP): Mechanical Property and Microcosmic Structure

Jianwei Yue,[1] **Limin Zhao**,[2] **Baoxi Zhang**,[1] **Qingmei Kong**,[2] **Siyuan Wang**,[1] **and Hao Wang**[1]

[1]*School of Civil Engineering and Architecture, Henan University, Kaifeng, Henan 475004, China*
[2]*Key Laboratory for Safety Evaluation and Restoration of Immovable Cultural Relics in Kaifeng City, Henan University, Kaifeng, Henan 475004, China*

Correspondence should be addressed to Limin Zhao; mumu55882005@163.com

Received 23 January 2021; Accepted 16 October 2021; Published 15 November 2021

Academic Editor: Santiago Garcia-Granda

The silty clay in the lower reaches of the Yellow River is characterized by loose structure, low strength, and strong capillary effect. Based on the technology of ancient glutinous rice mortar and microbial-induced calcium carbonate precipitation (MICP), experiments on optimal mass ratio of cementitious liquid to bacterial liquid and optimal concentration of cementitious liquid for MICP and improved MICP technology were carried out by measuring the production of $CaCO_3$, and direct shear test and unconfined compressive strength test of plain silt, glutinous mixing silt, and improved silt with MICP and modified MICP were conducted. The microstructure of the reaction products of MICP and improved MICP technology were also evaluated based on scanning electron microscopy (SEM). Research results showed that the mechanical properties of silt with glutinous rice slurry were effectively improved. With the increase in the concentration of glutinous rice slurry, the strength and internal friction angle of soil samples first increased and then decreased, and the cohesion presented a linear increasing trend. When the concentration of cementitious liquid was 0.5 M and the mass ratio of cementitious liquid to bacterial liquid was 2 : 1, the amount of $CaCO_3$ formed was the most, and the conversion rate of Ca^{2+} was more than 80%. The improved MICP could increase the conversion rate of Ca^{2+} (93.44%). An improved MICP showed that glutinous rice slurry could improve bacterial activity, increase the urease content in the bacterial solution, and promote the production of $CaCO_3$. Silt cohesion and internal friction angle of the silt were improved by the improved MICP technology, and the strengthening effect of mechanical properties of modified MICP-reinforced soil is better than that of the MICP-reinforced soil; conventional MICP technology could also improve the soil cohesion, but the improvement in the internal friction angle was not obvious. The SEM results indicated that compared with the reaction product of MICP technology, the structure of the product of improved MICP technology is more compact, resulting in a marked reinforcement of MICP performance with glutinous rice slurry. This study provides new insights into enhancing the mechanical behaviour of MICP-treated silt in the Yellow River Basin with glutinous rice slurry.

1. Introduction

Soil stabilization or soil strengthening is the process whereby soils are made stronger and more durable. Physical, biological, or chemical methods can be used. Cement has been widely used in foundation treatment for a long time [1]. However, the demand for alternative materials to cement is increasing because of its contribution to CO_2, SO_2, and NOx emission during production processes [2]. The environmental problems related to chemical or traditional soil additives were summarized by Al-Bared et al. [3]. In addition, more studies were provided on stabilizing soils using

environmentally friendly materials. Several innovative and sustainable green soil improvement techniques were introduced for geotechnical applications [4]. There are humongous amounts of bacteria in soil, which generate various biochemical products such as biofilms, various gases (e.g., N_2, CO_2, NO, H_2, and H_2S), biopolymers, or biominerals. Therefore, the direct use of in situ microbial activities or ex-situ microbial products has been proposed as a potential soil improvement method with a low environmental impact [5]. Microbial-induced calcium carbonate precipitation (MICP) is a technology, which has been emerging in recent years, which uses bacteria to induce calcium carbonate precipitation and thus has very good cementation and reinforcement effect on sandy soil and silty soil [6–8].

The MICP method has been investigated for improving various soil properties, including strength and stiffness [9, 10], liquefaction resistance [11, 12], wind/water erosion control [13], and permeability [14, 15]. The concentration of cementitious liquid affects the unconfined compressive strength of the treated soil. A high concentration of $CaCl_2$ is not conducive to urea hydrolysis and calcium carbonate deposition, while a low concentration of $CaCl_2$ is conducive to the reaction [16]. The calcium ion conversion rate is the highest when the cementitious liquid is 0.5 M. Calcium source and Ca^{2+} concentration have a direct effect on MICP. 0.25 M $CaCl_2$ can induce the highest calcium carbonate deposition efficiency [17]. The same concentrations of $CaCl_2$ and urea have a good mineralization effect, and a high concentration of cementing fluid will inhibit the mineralization reaction [18]. In current research and applications, multiple injections of bacteria and reaction solutions are still necessary to achieve the appropriate effect, which leads to long mineralization time, harmful intermediate products, etc., thereby, resulting in environmental pollution and disadvantages in the mineralization process [10, 19].

In ancient China, the composite material of the glutinous rice mortar was often used in the construction of city walls [20–23]. The components of glutinous rice have a similar function to that of organic matter in the process of biomineralization, the modified glutinous rice mortar has good initial fluidity, controllable setting time, and high early strength, and travertine particles form the calcium carbonate "crystal nucleus", which can provide a stable adhesion environment [24]. It is proved that the surface hardness, compressive strength, and splitting tensile strength of the treated soil could be affected by mixing a concentrated glutinous rice paste [25]. Liu et al. have obtained calcium carbonate crystals with various morphologies by using glutinous rice slurry as an organic control material and carbon source of carbon dioxide. The influence of the concentration of Ca^{2+} and reaction time on the morphology and polymorph of $CaCO_3$ crystals was researched to reveal the mechanism of MICP [26]. The combination of glutinous rice slurry and calcium carbonate can further strengthen the mechanical properties of soil [27–30].

In history, the Yellow River always burst its banks and caused severe floods, which makes the silt rich in organic matter and soluble salts, which makes it easy for bacteria to survive. In this paper, an improved MICP technology was proposed by introducing glutinous rice slurry into the MICP technology. The mechanical properties of the modern glutinous rice mortar, which consists of glutinous rice slurry, bacterial liquid, cementitious liquid, and calcium carbonate precipitation, were studied. Glutinous rice slurry can provide nutrients for microorganisms, and then improve the activity of microorganisms.

The primary objectives of this work are to investigate the effects of the glutinous rice slurry on the MICP technology. On one hand, glutinous rice pulp can provide a nutrient source for microorganisms and improve microbial activity; on the other hand, the combination of glutinous rice slurry and calcium carbonate forms a glutinous rice mortar, which further strengthens the mechanical properties of soil. The mechanical properties of the MICP-treated silt, the microstructure of the specimen, and the interactions between the glutinous rice slurry and microorganisms were investigated and analysed using the direct shear test, unconfined compressive strength, and scanning electron microscopy (SEM). It is a potentially environmentally friendly technique, while improving the foundation bearing capacity of soil.

2. Materials and Methods

2.1. Soil Preparation and Analysis. The research soil is selected from the Puyang City in the Yellow River area. Puyang City soil is mostly silt soil formed by the Yellow River flood and alluvial with poor water stability, strong water capillary effect, high strength when dry, but significantly reduced when wet [31]. The bearing capacity characteristic value of foundation soil before and after improvement is calculated with regard to the code for design of building foundation [32]. The basic physical properties of the soil used in this study are shown in Table 1. The basic physical property indexes of the research soil were measured according to the standard for the geotechnical testing method (GB/T 50123-2019) [33]. The grain size distribution of the site soil is presented in Figure 1, which are analysed through the particle grading test.

The silt was taken from 2 m underground. The soil samples are made according to the optimal moisture content and 96% compactness. The design dry density is 1.6 g/cm^3, and the moisture content is 17%.

Direct shear test: the diameter of the ring cutter sample is 61.8 mm, height is 20 mm, and volume is 60 cm^3. The theoretical weight of the ring cutter sample is 112.32 g, and the water content is 16.32 g. The sample is made and put it into the box for sealing and curing for 7 days.

Unconfined compressive strength test: a strain-controlled unconfined compression instrument was used. The soil sample is prepared by the mold of the triaxial test, and the sample size is $\Phi 38 \times 76$ (mm), volume is 86.193 cm^3, theoretical mass of one sample is 161.35 g, and theoretical water addition is 27.43 g. The prepared samples are added with a layer of fresh-keeping film and then put into the box for curing. Three samples are required for a group of unconfined tests. The compression test is carried out after 7 days of sealing and curing.

Table 1: Basic physical property indexes of soil particles in the Puyang area of the northeast Henan province.

Physical indicators	Nonuniform coefficient C_U	Coefficient of curvature C_C	Liquid limit WL_{17}	Plastic limit W_P	Optimum moisture content (%)	Maximum dry density ($g \cdot cm^{-3}$)
Plain soil	4.029	0.8281	29.82	16.52	16.94	1.671

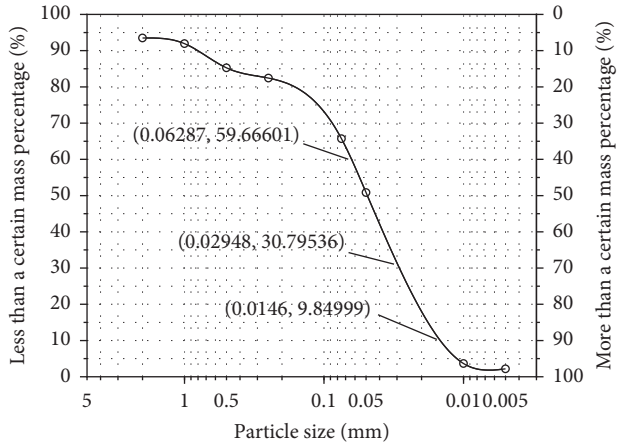

Figure 1: The grain size distribution of the soil.

2.2. Glutinous Rice Slurry. Glutinous rice slurry: commercial pulverized sticky rice was used in this study. The pulverized sticky rice was purchased from the local market in Kaifeng city of Henan province, which are food grade materials. The amylose content in the rice starch ranges from 0.9 wt. % to 1.1 wt. % with a protein content of around 7.6 wt. %. The glutinous rice powder is mixed with distilled water to prepare slurry with a concentration of 1%, 3%, 5%, 7%, and 9%. Glutinous rice flour of different qualities is cooked with water and high pressure to prepare glutinous rice pulp with a concentration of 1%, 3%, 5%, 7%, and 9%. The preparation method of the glutinous rice pulp with 1% concentration is as follows: wash and dry the conical flask, add 1 g glutinous rice flour into the bottle, add tap water to the bottle to 100 g, and seal the bottle mouth with air permeable materials such as newspaper, and then put it into an electric rice cooker to heat and boil for at least 4 h [34] (refer to this for other concentrated glutinous rice paste). During the process, write down the scale of the electric rice cooker and add an appropriate amount of water to keep the consistency of glutinous rice slurry unchanged [35–37].

2.3. Preparation and Treatment of Bacteria. This study utilized Sporosarcina pasteurii ATCC 11859 purchased from Shanghai Bioresource Collection Center.

3. Improved Material and Their Properties

3.1. Experiment on Improved Silt with Glutinous Rice Slurry

3.1.1. Mechanical Properties of Improved Silt. To verify the effectiveness of glutinous rice slurry in improving the soil properties, 1%, 3%, 5%, 7%, and 9% glutinous rice slurry was mixed to the soil evenly. Then, the sample was cured for 7 days in the sealing box.

(1) Direct Shear Test Under Low Stress. The number of floors of rural buildings in the Yellow River region is low, and the actual vertical pressure is often lower than that of high-rise buildings [38]. In this paper, the vertical stress is 50 kPa, 100 kPa, 150 kPa, and 200 kPa, respectively. According to the standard of geotechnical test methods [33], direct shear tests were carried out. The shear stress and shear displacement of the improved soil samples are shown in Figure 2.

It can be seen from Figure 2 that with the increase in the vertical stress, the shear stress increases. With the increase in the concentration of glutinous rice slurry, the shear strength of the samples first increases and then decreases. It can be seen that different concentrations of glutinous rice slurry have different effects on the improvement of the sample. The 3% glutinous rice slurry samples show a good shear strength performance. The sample without glutinous rice slurry has lower peak strength and later strength. The sample with glutinous rice slurry shows a better performance under lower stress, which indicates that glutinous rice slurry is more suitable for engineering under low-stress conditions. According to the shear strength of the samples under different glutinous rice slurry content, the relationship curve between the shear strength and vertical stress is fitted, as shown in Figure 3.

Figure 3 shows that with the increase in the glutinous rice slurry content, the shear strength of samples first increases and then decreases. When the glutinous rice slurry content is 3%, the internal friction angle is the largest. In addition, when the glutinous rice slurry content is 9%, the cohesion is the largest. The cohesion and internal friction angle of the samples under different glutinous rice slurry

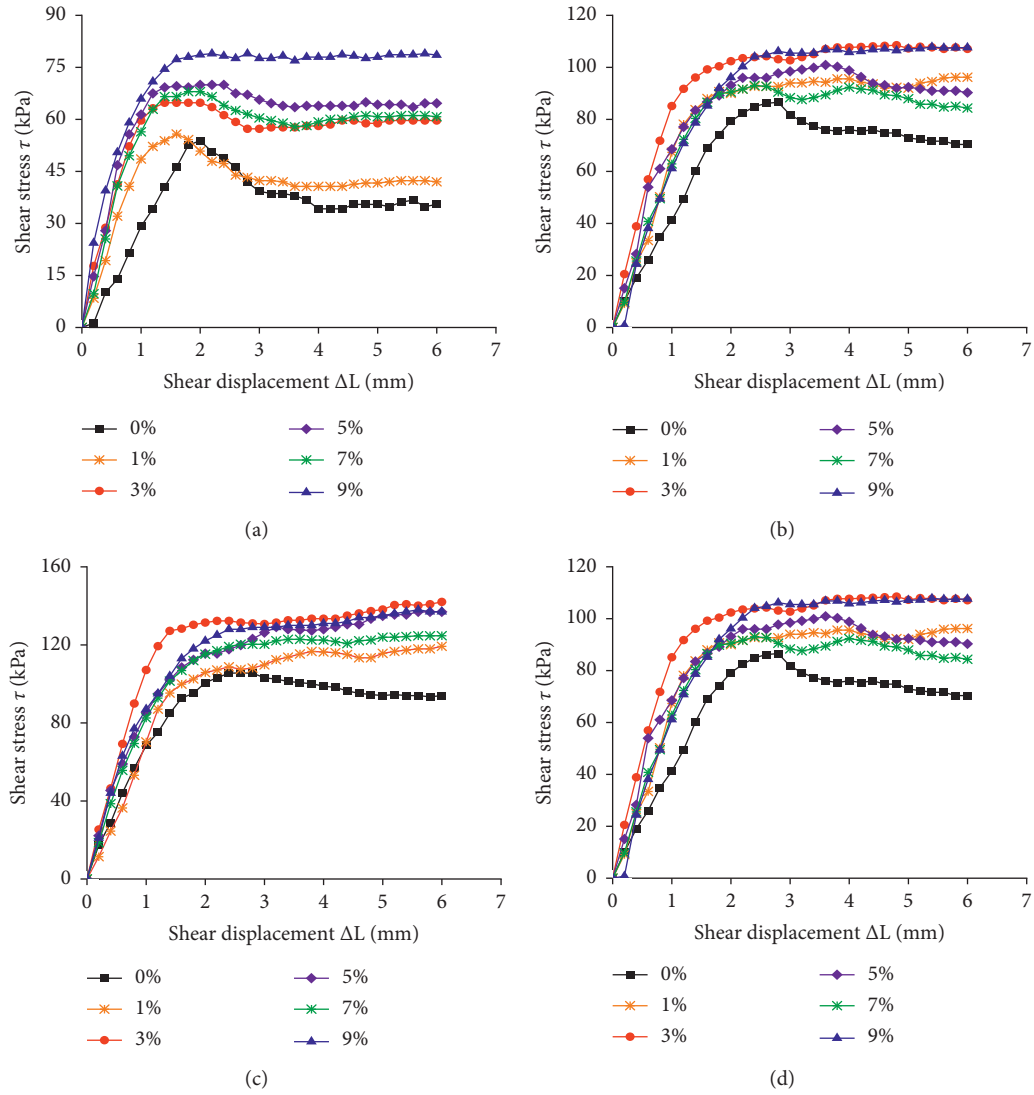

Figure 2: Shear stress and shear displacement curves of samples at different concentrations of glutinous rice slurry. (a) Vertical stress—50 kPa. (b) Vertical stress—100 kPa. (c) Vertical stress—150 kPa. (d) Vertical stress—200 kPa.

contents are shown in Figure 4. With the increase in the content of glutinous rice slurry, the internal friction angle first increases and then decreases, and the cohesion increases linearly. The reason for this phenomenon is that the pores between the soil particles are gradually filled with glutinous rice slurry, which improves the cohesion between particles [39, 40].

However, with the continuous increase in the glutinous rice slurry content, excessive glutinous rice slurry adheres to the surface of soil particles, resulting in the decrease of frictional force between particles and the decrease of the internal friction angle.

(2) Unconfined Compressive Strength Test. The unconfined compressive strength can reflect the relationship between the mechanical properties of the specimen and the improved materials. According to the standard of geotechnical test methods [41], the unconfined compressive strength test of the specimens was carried out by using the strain-controlled unconfined compression instrument at the axial strain rate of 1 mm/min. The relationship between axial stress and strain of specimens at different concentrations of glutinous rice slurry is shown in Figure 5.

It can be seen from Figure 5 that with the increase in the glutinous rice slurry content, the maximum axial stress of the samples first increases and then decreases. When the concentration of glutinous rice slurry is 3%, the axial stress reaches the maximum value, that is, the unconfined compressive strength reaches the maximum value. The unconfined compressive strength (i.e., antideformation ability) of the samples with glutinous rice slurry solution is significantly improved. The unconfined compressive strength of the samples increased by 19.3%, 60.5%, 43.7%, 35.8%, and 32.1%, respectively, with 1%, 3%, 5%, 7%, and 9% glutinous rice slurry, respectively, and the deformation resistance of the samples increased by 11.9%, 33.9%, 44.9%, 55.9%, and 78.8%, respectively. It can be seen that the strength of the samples is related to the content of the glutinous rice slurry,

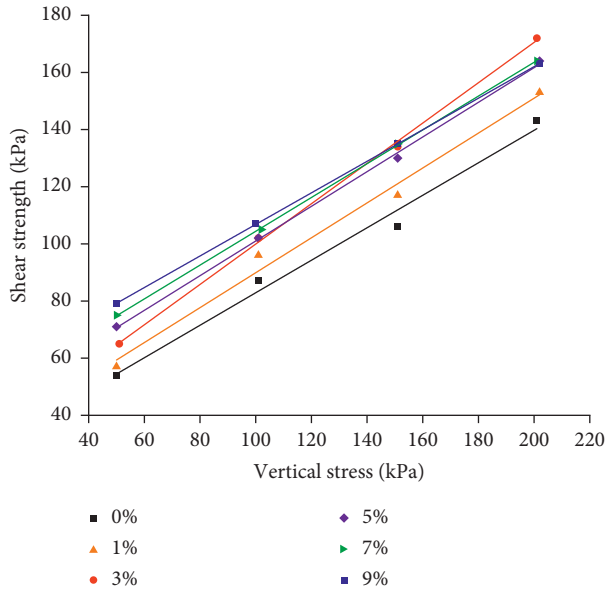

Figure 3: Shear strength vs. vertical pressure curve of samples at different concentrations of glutinous rice slurry.

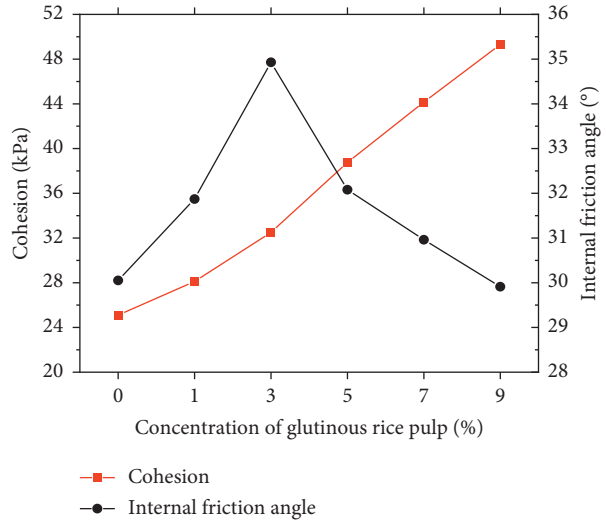

Figure 4: Variation of cohesion and internal friction angle of samples with different glutinous rice pulp concentrations.

and the improvement effect of different contents of glutinous rice slurry on the sample is different.

3.2. Cultivation, Improvement, and Activity of Microorganisms

3.2.1. Microbial Cultivation and Improvement. The 1 L microbial liquid culture medium formula is shown in Table 2 [42].

3.2.2. Microbial Activity. The OD_{600} value of bacteria reflects the bacterial activity [42, 43]. The higher the activity of the bacterial liquid, the lower the transmittance is, which

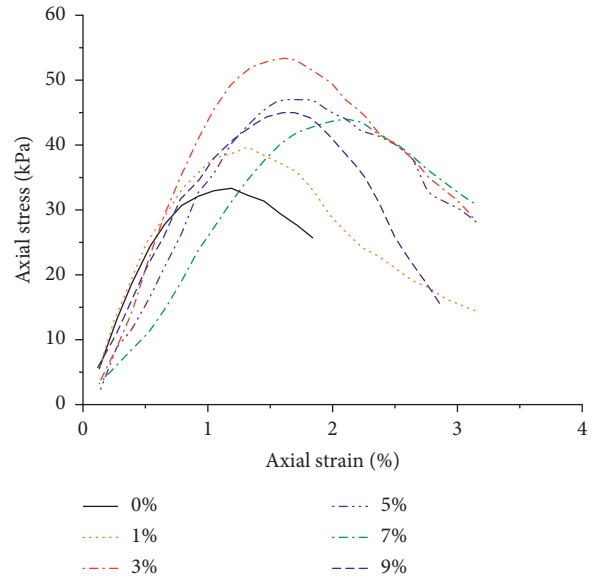

Figure 5: Axial stress and strain curves of samples with different glutinous rice pulp concentrations.

indicates that the OD_{600} value of the bacterial liquid is higher. The formula of the three groups of the bacterial liquid is shown in Table 2, of which group I is a common bacterial liquid, group II is a modified bacterial liquid, and group III is a bacterial liquid containing 3% glutinous rice slurry. The OD_{600} value of group I is 1.542, that of group II is 1.836, and group III is 0.405. The activity of group II was increased by 19% compared to that of group I, which indicated that the amount of urease in improved microbial metabolism was higher than that of the common bacterial solution; the activity of group III was lower than that of group I and II, but it also showed that glutinous rice slurry could provide nutrition for bacteria and increase the activity and concentration of bacteria.

3.2.3. Optimal Ratio of Calcium to Bacteria for MICP. The mass ratio of cementitious liquid to bacterial liquid is shown in Table 3. The optimal mass ratio of cementitious liquid to bacterial liquid was studied by measuring the production of $CaCO_3$. The test was divided into two groups A–F and a–f, as shown in Figure 6. Group A–F was dried and weighed after filtration, and group a–f was dried and weighed directly. The residual solid after drying is shown in Figure 7. It can be seen from Figure 7 that there are more brown solids in group A, B, and C after drying, and more white solids appear in group C to group F, but many white $CaCl_2$ crystal substances appear on the surface of group F. Therefore, the remaining solids after drying include bacteria, $CaCO_3$ precipitation, and $CaCl_2$ crystals, which were not completely reacted.

MICP is to convert Ca^{2+} into $CaCO_3$ precipitation. After filtration and drying of group A~F, the concentration of the calcium ion was measured by the EDTA standard solution titration method [44], and the actual amount of $CaCO_3$ precipitation can be measured.

Table 2: Medium formulation of Bacillus pasteurella.

Group	Yeast powder (g/L)	Peptone (g/L)	Sodium chloride (g/L)	Urea (g/L)	Glutinous rice slurry	Agar
I	5	10	10	10	0	30
II	5	10	10	10	30	30
III					30	0

Table 3: Experimental groups with different mass ratios of cementitious liquid to bacterial liquid.

Group	A/a	B/b	C/c	D/d	E/e	F/f
The mass ratio of cementitious liquid to bacterial liquid	0.25 : 1	0.5 : 1	1 : 1	2 : 1	3 : 1	4 : 1
Cementitious liquid (M)	0.5	0.5	0.5	0.5	0.5	0.5
Cementitious liquid (g)	1.92	3.2	4.8	6.4	7.2	7.68
Bacterial liquid (g)	7.68	6.4	4.8	3.2	2.4	1.92
Total	9.6	9.6	9.6	9.6	9.6	9.6

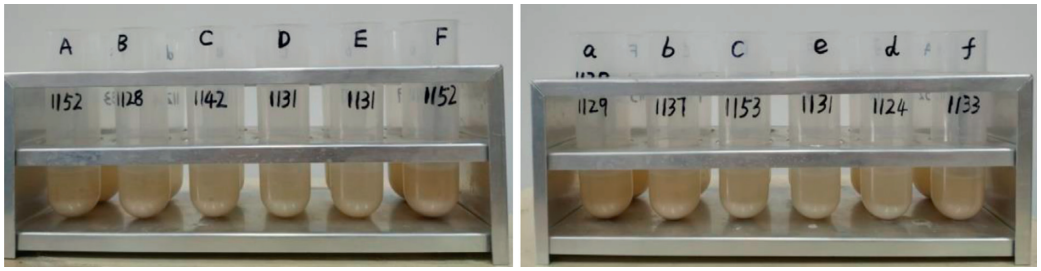

Figure 6: Reaction phenomenon under different mass ratios of cementitious liquid to bacterial liquid.

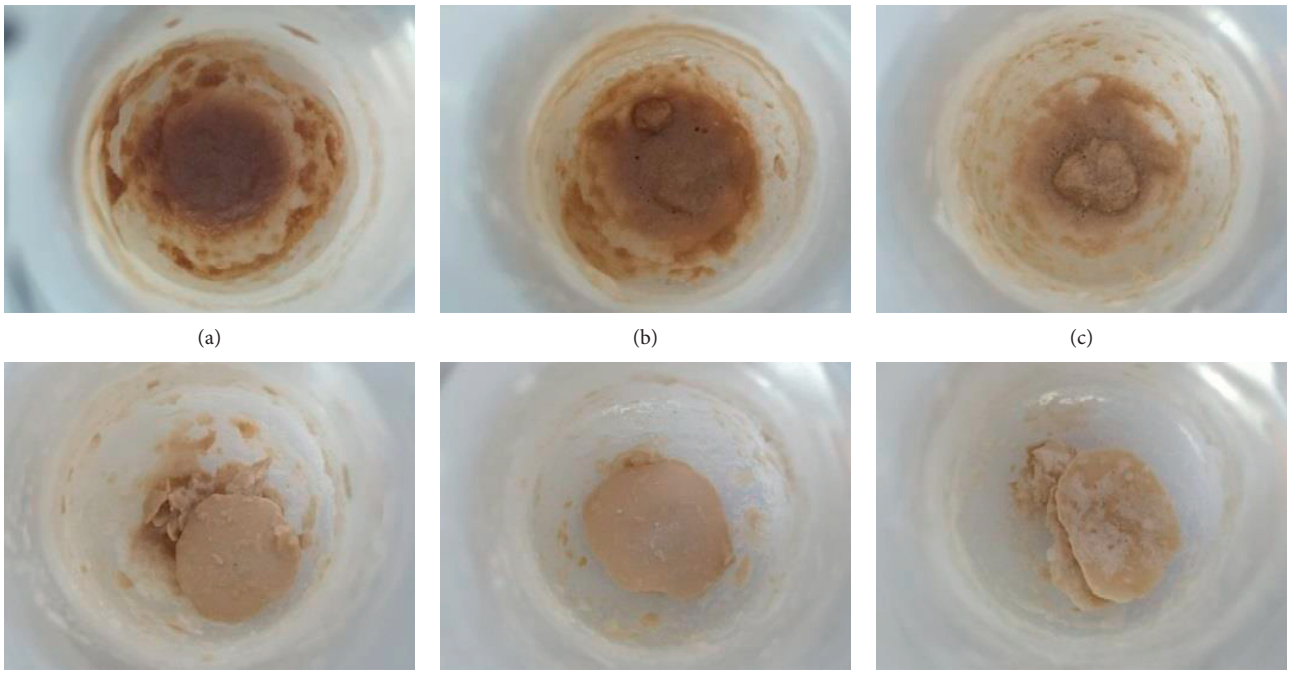

Figure 7: Residual solids under different mass ratios of cementitious liquid to bacterial liquid. (a) Group (0.25 : 1). (b) Group (0.5 : 1). (c) Group (1 : 1). (d) Group (2 : 1). (e) Group (3 : 1). (f) Group (4 : 1).

The concentration of calcium ion and the mass of calcium carbonate precipitation were calculated as follows:

$$\begin{aligned} C\left(Ca^{2+}\right) &= V(\text{EDTA}) \cdot c(\text{EDTA}), \\ M\left(CaCO_3\right) &= c\left(Ca^{2+}\right) \cdot V(\text{HCl} + \text{NaOH}) \cdot M\left(CaCO_3\right), \end{aligned} \tag{1}$$

where c (Ca^{2+}) is the concentration of the calcium ion (mol/L), V (EDTA) is the amount of the EDTA standard solution (ML), c (EDTA) is the concentration of the EDTA standard solution (mol/L), taking 0.1 mol/L, V (HCl + NaOH) is the total volume of hydrochloric acid and sodium hydroxide dropping (ml), M ($CaCO_3$) is the amount of calcium carbonate, taking 100, and m ($CaCO_3$) is the mass of calcium carbonate (g).

By measuring the amount of $CaCO_3$ precipitation in group A~F, it was found that the conversion rate of Ca^{2+} in group A~D was 83.22%, 76.69%, 74.16%, and 80.69%, respectively. The amount of $CaCO_3$ precipitation increased gradually, which were 0.0799 g, 0.1227 g, 0.178 g, and 0.258 g, respectively. The conversion rate of Ca^{2+} in Group E and F was 43.30% and 26.95%, respectively, and the precipitation amount of $CaCO_3$ was 0.1559 g and 0.1035 g, respectively. The actual mass of $CaCO_3$, the solid content after filtration and drying, the amount of residual solid after drying, and the conversion rate of Ca^{2+} are shown in Figure 8. It can be seen that group D produces the most $CaCO_3$, and the conversion rate of Ca^{2+} is more than 80%, which is the best mass ratio of cementitious liquid to bacterial liquid.

3.2.4. Optimal Concentration of Cementitious Liquid for MICP. The optimal concentration of cementitious liquid for MICP technology was studied with the best mass ratio of cementitious liquid to bacterial liquid (2 : 1). The experimental cementitious liquid concentrations were 0.25 M, 0.5 M, 0.75 M, 1.0 M, 1.5 M, and 2.0 M, respectively. The mass of different cementitious liquid and bacterial liquid is shown in Table 4.

The experiment was conducted in G–L and g–l groups, as shown in Figure 9. After filtration and drying, the G~L group was titrated with EDTA standard solution [45], and the g–l group was dried for observation. The residual solids after drying are shown in Figure 10. The actual mass of $CaCO_3$, the amount of residual solid after drying, and the conversion rate of Ca^{2+} are shown in Figure 11. In Figure 9, white precipitates can be observed in G/g and H/h, but no obvious precipitation was found in the other four groups, which is mainly due to the inhibition of urease induced ions by a high concentration of cementitious liquid, thus affecting the formation of $CaCO_3$.

It can be seen from Figure 10 that there are more white solid precipitates after drying in groups g and h; the solid colour in groups i and j are yellowish after drying, and many white $CaCl_2$ crystal substances appear on the solid surface after drying in groups K and l, which are mainly caused by the high concentration of the cementitious liquid. The remaining substances in group i – 1 after drying are bacteria, calcium chloride, and a small amount of calcium carbonate. The results showed that the conversion rate of Ca^{2+} in group G and group H was 83.94% and 82.19%, respectively. The precipitation of $CaCO_3$ was 0.1343 g and 0.263 g. The conversion rate of Ca^{2+} in group i – l decreased from 73.44% to 34.79%, but the amount of $CaCO_3$ increased slowly.

The best calcium concentration (0.5 M) was obtained by the experiment of the best mass ratio of cementitious liquid and bacteria liquid. When the concentration of cementitious liquid was 0.5 M and the mass ratio of gum fungus was 2 : 1, the conversion rate of Ca^{2+} and the production of calcium carbonate were the highest. Based on this ratio, glutinous rice slurry was introduced to improve the MICP technology.

3.2.5. Research on Improved MICP Technology. Based on the optimal calcium concentration (0.5 M), the optimal mass ratio of cementitious liquid to bacterial liquid (2 : 1) and improved bacterial liquid, the $CaCO_3$ production under the improved MICP technology was studied. The mass of improved bacterial solution and cementitious liquid is shown in Table 5.

The test was divided into two groups M and m as shown in Figure 12. After filtration and drying, group M was titrated with EDTA standard solution. The actual amount of $CaCO_3$ precipitated was 0.299 g, and the conversion rate of Ca^{2+} was 93.44%. The remaining solids in group M after drying are shown in Figure 13. The white solid material was white with a few transparent flakes, which were preliminarily judged as the state of glutinous rice slurry after drying.

After improvement, the Ca^{2+} conversion rate of group M was 12.75% higher than that of group D and 11.25% higher than that of group h. These results indicated that the modified MICP can help to increase the concentration of bacteria, thus increasing the urease content in the bacterial solution and promoting the production of $CaCO_3$. Comparing group M, group D, and group H, it was found that group M had one more layer of slurry film than the other two groups after drying. The film and $CaCO_3$ were beneficial to improve the adhesion between particles, which indicated that glutinous rice slurry played a favourable role in traditional earthen sites.

3.2.6. SEM Scanning Electron Microscopy. The solid materials (bacteria, $CaCO_3$ precipitation, $CaCl_2$ crystal, and glutinous rice slurry) in group a–m and $CaCO_3$ particles produced by $CaCl_2$ and Na_2CO_3 reaction products were scanned by SEM to observe the shape, structure, and other properties of the $CaCO_3$ solid substances induced by Bacillus Pasteurella, as shown in Figures 14–16.

The left side of Figures 14–16 shows the microscopic diagram of solid matter under 1000 times magnification, and the right side of Figures 14–16 shows the microscopic diagram of solid matter with a magnification of 5000 times. The results of scanning electron microscopy showed that in the group a–f, $CaCO_3$ precipitated less in groups a and b, and more bacteria were wrapped in $CaCO_3$ particles; in group c, CaCO3 precipitation began to increase, but many bacteria could still be observed; group d had the most $CaCO_3$ precipitation and fewer bacteria; groups e and f had less $CaCO_3$

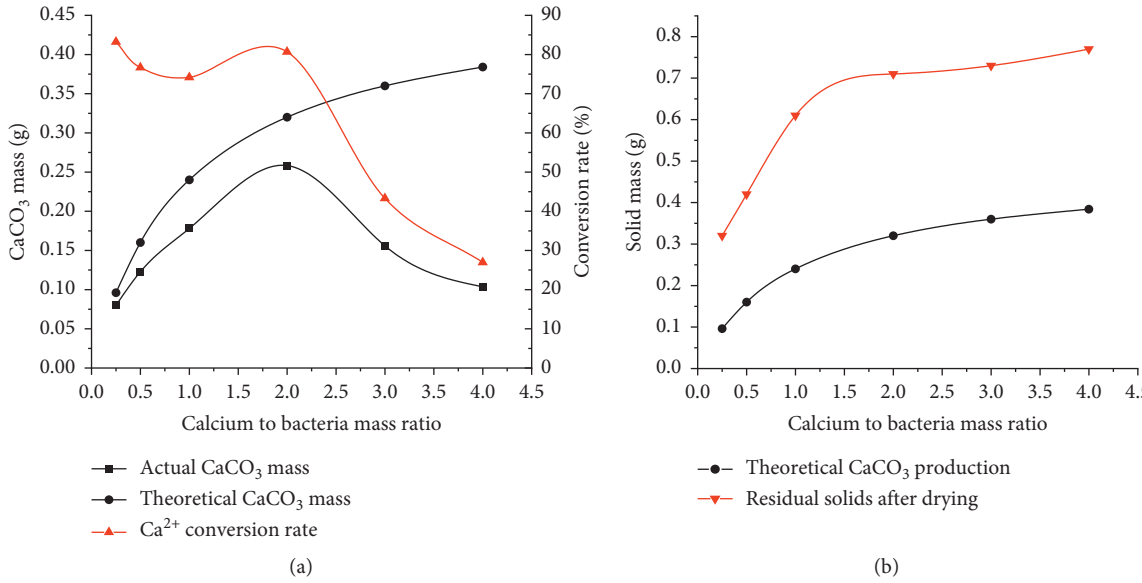

Figure 8: Changes in $CaCO_3$, Ca^{2+} conversion rate, and residual solid content under different mass ratios of cementitious liquid to bacterial liquid. (a) $CaCO_3$ mass. (b) Residual solids mass under calcium to bacteria mass ratio.

Table 4: Experimental groups with different cementitious liquid concentrations.

Group	G/g	H/h	I/i	J/j	K/k	L/l
The mass ratio of cementitious liquid to bacterial liquid	2 : 1	2 : 1	2 : 1	2 : 1	2 : 1	2 : 1
Cementitious liquid (M)	0.25	0.5	0.75	1.0	1.5	2.0
Cementitious liquid (g)	6.4	6.4	6.4	6.4	6.4	6.4
Bacterial liquid (g)	3.2	3.2	3.2	3.2	3.2	3.2
Total	9.6	9.6	9.6	9.6	9.6	9.6

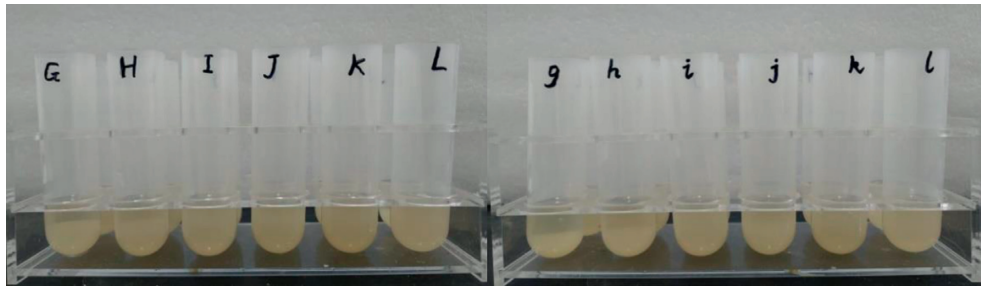

Figure 9: Reaction phenomenon under different calcium concentrations.

precipitation, and more $CaCl_2$ crystals were wrapped on $CaCO_3$ particles. In groups g–l, the conversion rate of Ca^{2+} in group g and group h was higher, and more $CaCO_3$ was visible; in group i–l, the conversion rate of Ca^{2+} decreased gradually, and a small amount of $CaCO_3$ and a large number of $CaCl_2$ crystals were attached to $CaCO_3$. Group *M* was added glutinous rice slurry based on group D and group h. Compared with group D and group H, more and more $CaCO_3$ particles can be seen in group M. On the one hand, the conversion rate of Ca^{2+} in group *M* was increased by 10% compared with that in group D and H; on the other hand, glutinous rice slurry envelops $CaCO_3$ particles and formed a layer of invisible film on its surface. Comparing the three groups of samples D, H, and M in Figure 14 with those in Figures 15 and 16, their similarity was very high, which proved that they were $CaCO_3$ particles. Because $CaCl_2$ crystals were attached to the surface of group D and h, and glutinous rice slurry was attached to the surface of group *M*, the SEM images of the three groups of samples were slightly different from those of $CaCO_3$ particles. Previous studies have shown that the reduction in the void space due to the $CaCO_3$ precipitation is considered to be a primary strengthening factor in the reduced brittleness behavior of the MICP-treated sand [44].

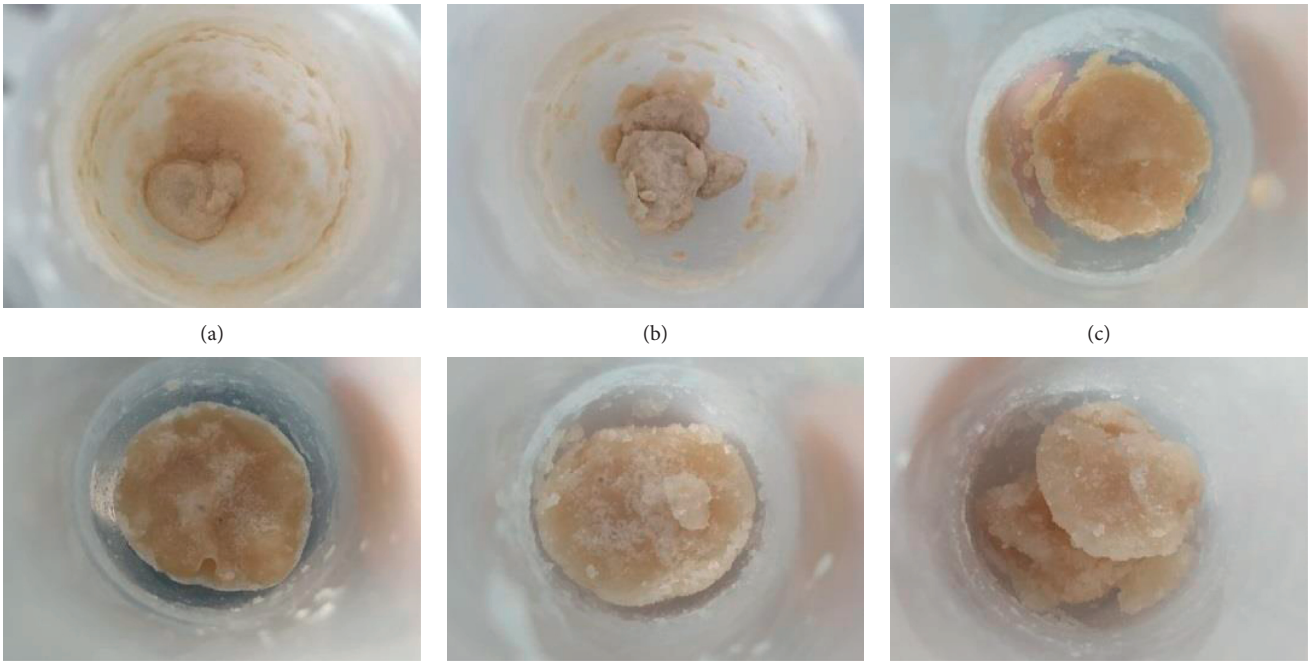

Figure 10: Residual solids under different calcium concentrations. (a) g group (0.25 M); (b) h group (0.5 M); (c) i group (0.75 M); (d) j group (1.0 M); (e) k group (1.5 M); (f) l group (2.0 M)

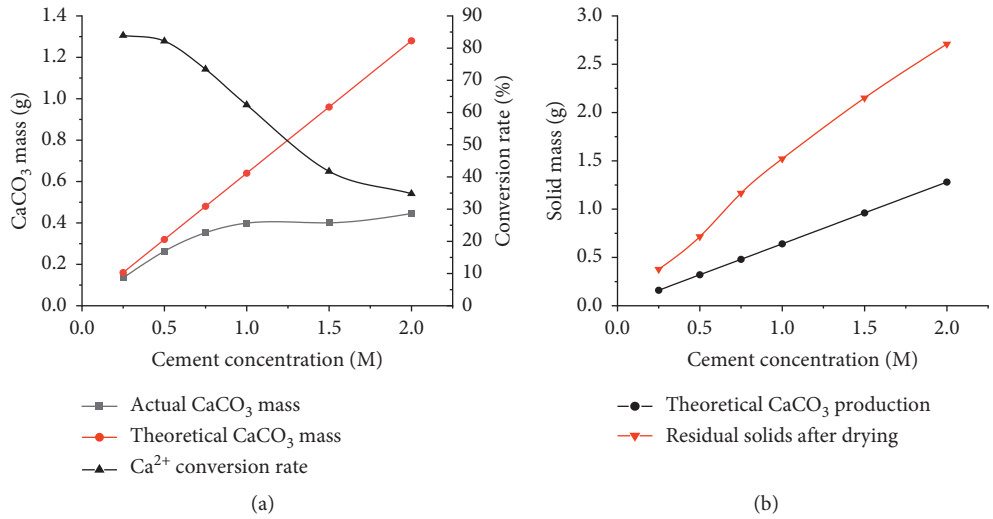

Figure 11: Changes in $CaCO_3$ and Ca^{2+} conversion rate and residual solid content at different calcium concentrations. (a) $CaCO_3$ mass. (b) Residual solid mass at calcium to bacteria mass ratio.

Table 5: Mass of calcium and bacterial liquid of improved MICP.

Group	Mass ratio of cementitious liquid to bacterial liquid	Concentration of improved cementitious liquid (M)	Cementitious liquid (g)	Improved bacterial liquid (g)
M/m	2 : 1	0.5	6.4	3.2

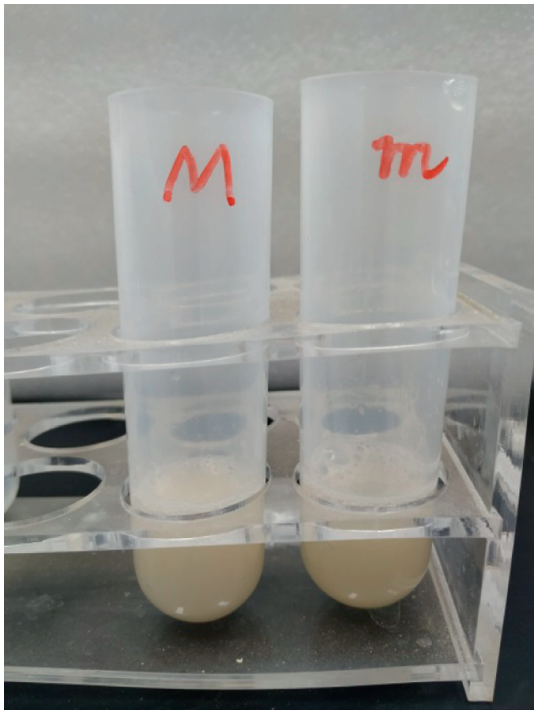

Figure 12: *M* and *m* groups with improved MICP.

Figure 13: Remaining solids in group with improved MICP.

4. Experimental Study on Mechanical Properties of Soil

4.1. Sample Preparation. MICP technology and improved MICP technology were introduced into plain soil by the mixing method. Three kinds of soil samples were prepared, namely, plain soil, MICP-reinforced soil, and improved MICP-reinforced soil. Three groups of samples were set, namely, pure water group, common bacterial liquid group, and 3% glutinous rice slurry improved bacterial liquid group. Direct shear test specimens were 61.8 mm in diameter, 20 mm in height, and 60 cm^3 in volume. Unconfined compressive strength test specimens were Φ 38 × 76 (mm) and 86.193 cm^3 volume. Based on 96% compaction (dry density of 1.6 g/cm^3), dry soil quality needed for a direct shear test piece was 112.32 g, and an unconfined specimen required dry soil quality of 161.35 g. With 17% moisture content, a direct shear needed pure water of 16.32 g and an unconfined specimen needed pure water of 27.43 g. In the common bacterial solution group, the bacterial solution was added by 1% solute removal method, and in the improved bacterial solution group with 3% glutinous rice slurry, the bacterial solution was added by 3% solute removal method, as shown in Figure 17. The amount of slurry added to a direct shear sample and an unconfined compressive sample is shown in Table 6.

It can be seen from Figure 17 that water permeability was faster in the pure water group (Figure 17(a)). The permeation rate of the common bacterial solution group (Figure 17(b)) was the second, and the water permeation rate was slow due to the reaction of the bacterial solution and cementing solution to form calcium carbonate precipitate. The infiltration rate of the modified bacteria liquid group with a concentration of 3% was the slowest (Figure 17(c)). The main reason was that the blocking effect of the glutinous rice paste and the reaction of the bacteria liquid with the cement liquid resulted in the formation of calcium carbonate precipitate, which made it difficult for water to enter the soil. According to the sample preparation method of the direct shear test and unconfined compressive strength test at different glutinous rice slurry concentrations, the prepared samples were put into a sealed box and cured for 7, 14, and 28 d. Some samples are shown in Figure 18.

4.2. Mechanical Test of Specimens

4.2.1. Direct Shear Test. Direct shear test under different vertical pressures is a kind of more convenient and quick determination of cohesion and friction angle of soil, which can directly reflect the soil mechanics performance.

The theoretical expression of soil strength is as follows [46]:

$$\tau = c + \sigma \tan \Phi, \tag{2}$$

where τ is the shear stress, σ is the normal stress, c is cohesion, Φ is the angle of internal friction, and $\sigma \cdot \tan\Phi$ represents internal friction.

The test process is in strict accordance with the standard of the soil test method [33]. The maintenance of specimens was done for 7 d, 14 d, and 28 d, respectively. Shear stress and displacement curve under different curing days are shown in Figure 19, and the shear rate is 0.8 mm/min. The results are shown in Table 7.

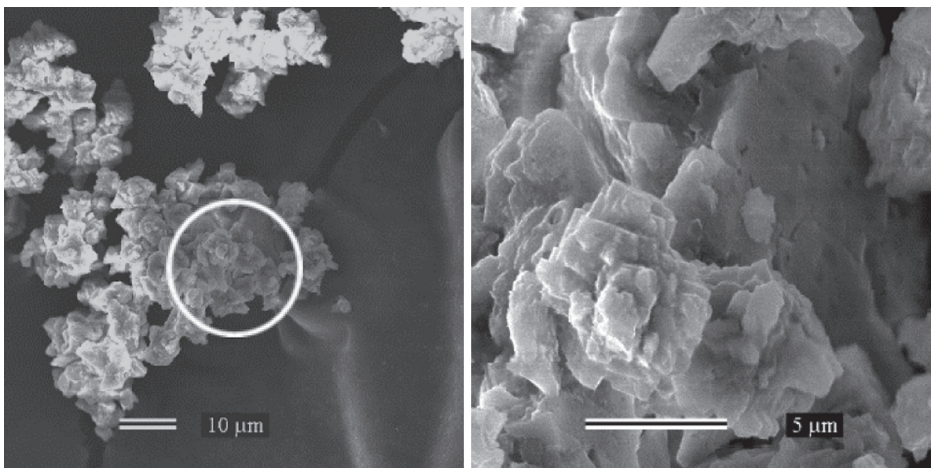

Figure 14: SEM of $CaCO_3$ particles.

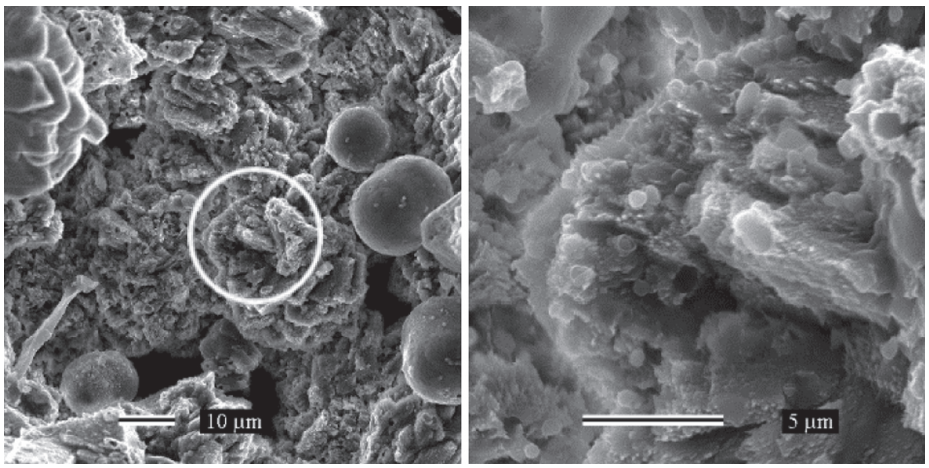

Figure 15: SEM of residual solid matter after drying in m group.

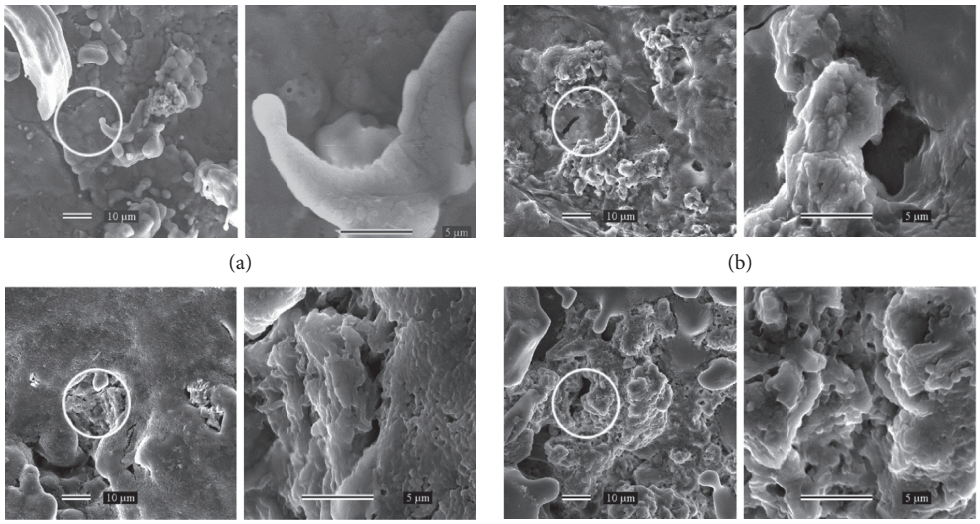

Figure 16: Continued.

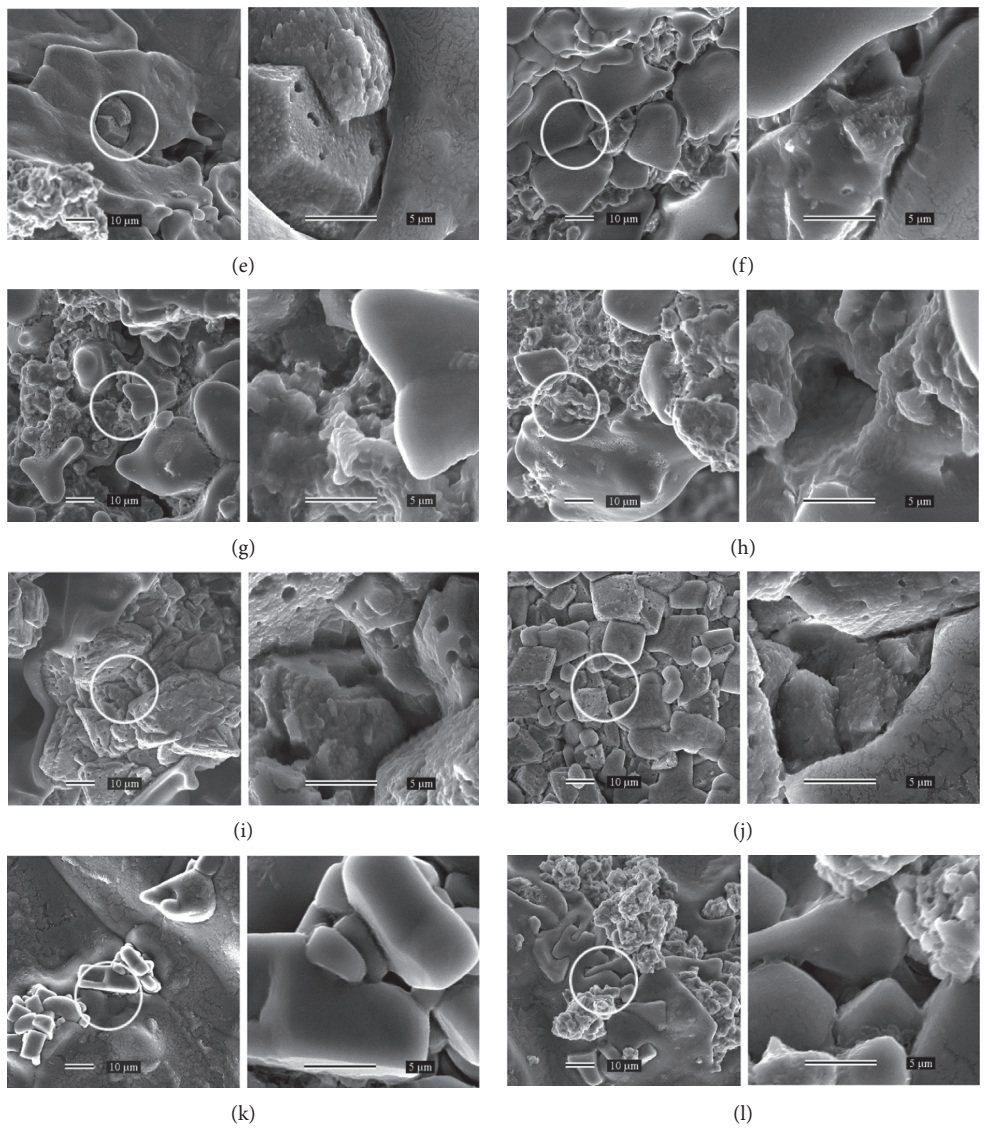

Figure 16: Scanning electron microscopy of residual solid matter in groups A–l after drying. (a) Group (0.25 : 1). (b) group (0.5 : 1). (c) Group (1 : 1). (d) Group (2 : 1). (e) Group (3 : 1). (f) Group (4 : 1). (g) Group (0.25 M). (h) Group (0.50 M). (i) Group (0.75 M). (j) Group (1.0 M). (k) Group (1.5 M). (l) Group (2.0 M).

Figure 17: Mixing of soil samples: (a) pure water group, (b) common bacterial solution group, and (c) improved bacterial solution group.

Table 6: Slurry amount of one direct shear specimen and one unconfined compression specimen.

Group	Serous category	Direct shear test (g)	Unconfined sample (g)
Pure water group	Water	16.32	27.43
Common bacterial solution group (2 : 1)	0.5 M cementing fluid	10.99	18.47
	Bacteria liquid	5.49	9.24
Improved bacterial solution group (2 : 1)	0.5 M modified cementing fluid	11.21	18.85
	Modified bacteria liquid	5.61	9.43

(a) (b) (c)

Figure 18: Curing diagram of the direct shear test and unconfined compressive strength test specimen: (a) plain soil, (b) MICP-reinforced soil, and (c) improved MICP-reinforced soil.

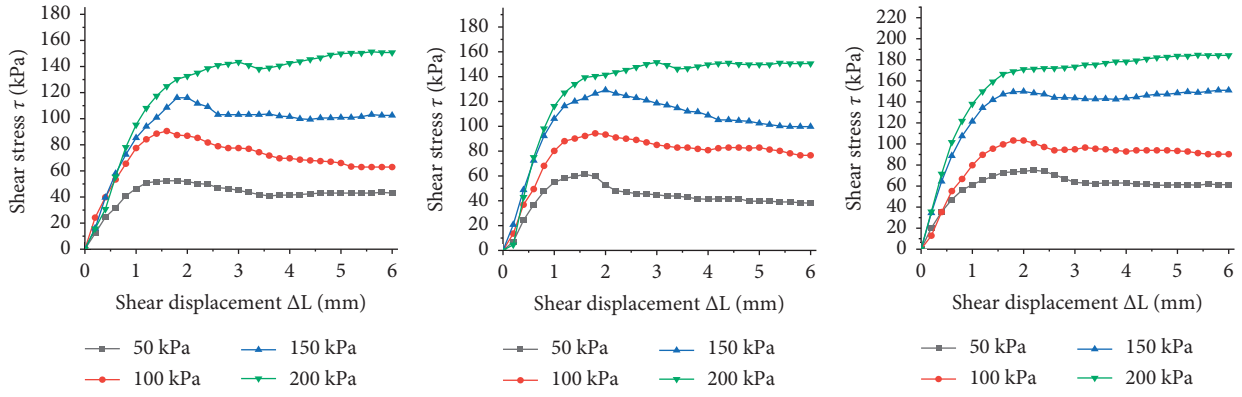

(a) (b) (c)

Figure 19: Continued.

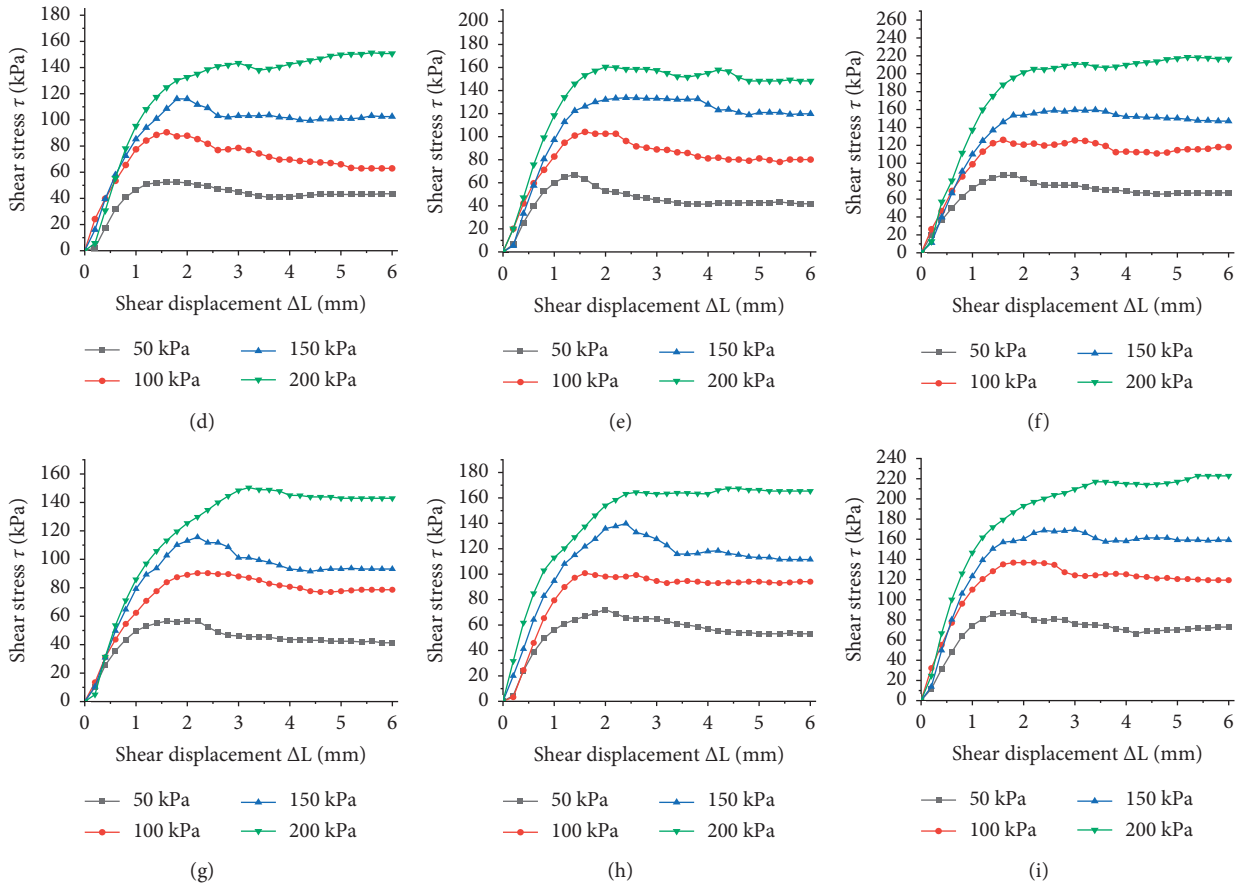

Figure 19: Curve of shear stress and shear displacement at different curing days. (a) Plain soil—7 d; (b) MICP-reinforced soil—7 d; (c) improved MICP soil—7 d; (d) plain soil—14 d; (e) MICP-reinforced soil—14 d; (f) improved MICP soil—14 d; (g) plain soil—28 d; (h) MICP-reinforced soil—28 d; and (i) improved MICP soil—28 d.

Table 7: Direct shear test results under different curing days.

Soil sample	Vertical pressure (kPa)	7 d shear strength (kPa)	14 d shear strength (kPa)	28 d shear strength (kPa)
Plain soil	50	52.9	52.4	56.6
	100	86.4	90.5	90.3
	150	110.8	116	115.6
	200	142.1	143.4	150.4
MICP-reinforced soil	50	61.3	67.1	72.1
	100	94.3	104.1	100.8
	150	129.1	133.7	139.8
	200	151.5	160.5	164.4
Improved MICP-reinforced soil	50	75.1	86.4	87
	100	103.3	126.1	136.8
	150	149.9	159.5	169.3
	200	178.2	210.7	217

The shear strength of the plain soil under different vertical pressures during the curing period of 7 to 14 d did not change too much, but the shear strength of the plain soil increased slightly after the curing period of 28 d. The main reason was that the moisture content of the sample decreased during the curing process, which led to an increase in the shear strength of the sample. When the curing time of soil strengthened by MICP and modified MICP was from 7 d to 14 d, the variation range of shear strength under different vertical pressures was larger than that under 14 d to 28 d. Under the same vertical pressure and different curing days, the shear strength of the three samples showed a step-type increase. According to formula (2), the relation curve between the shear strength and vertical pressure is fitted, as shown in Figure 20.

The relation curve between the shear strength and vertical pressure changed regularly for different curing days.

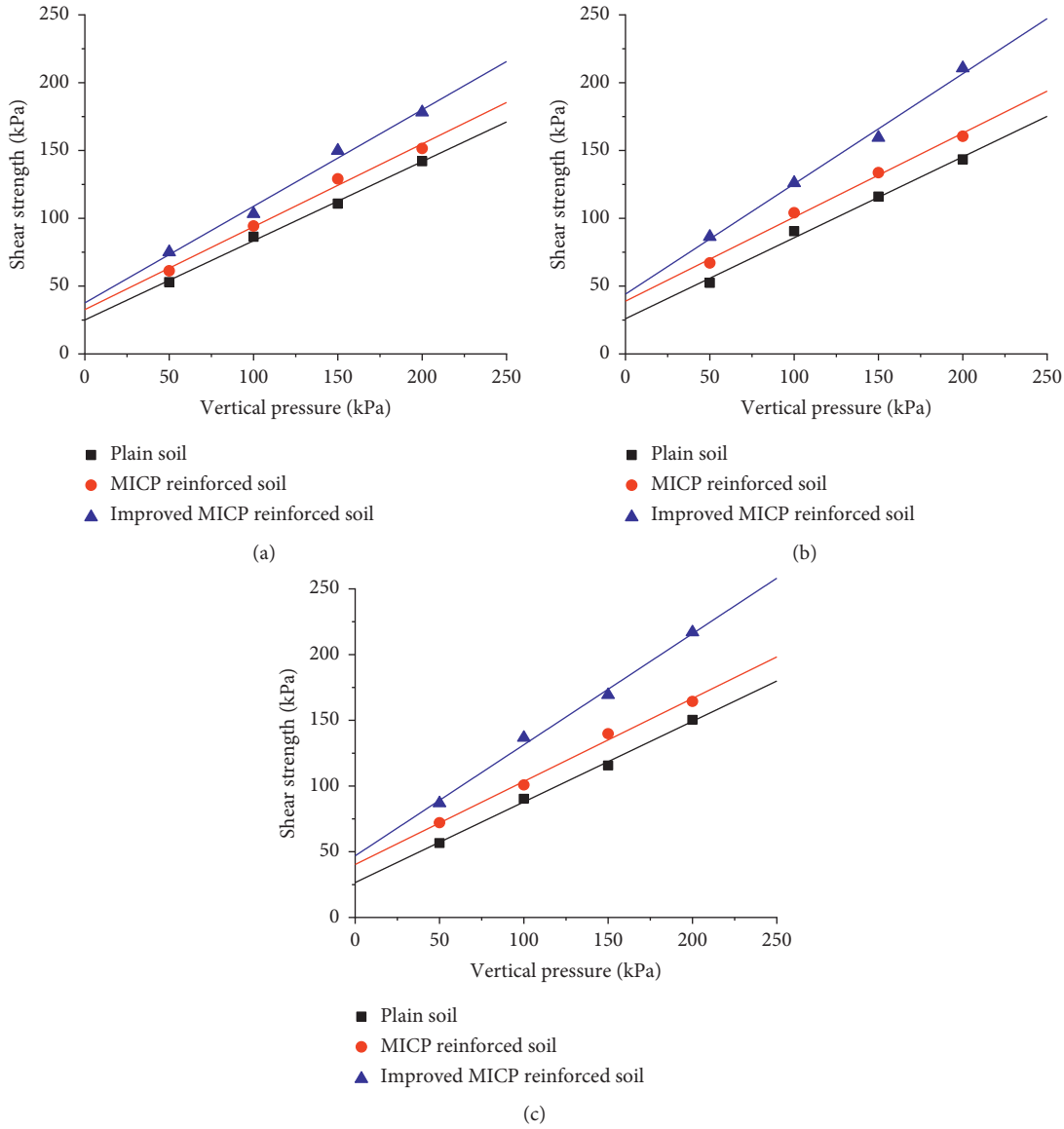

Figure 20: Relationship between shear strength and vertical pressure at different curing days. (a) Curing for 7 d; (b) curing for 14 d; and (c) curing for 28 d.

The Y-axis intercept of soil consolidated with improved MICP was the largest and increases with the increase in curing days. The Y-axis intercept of soil consolidated with MICP was larger than that of soil consolidated with plain soil. The slope of the soil consolidated with improved MICP was the largest and tends to increase with the increase in the curing days. The slope of the soil consolidated with MICP was similar to that of the plain soil and almost unchanged with the increase in the curing days. The cohesion and internal friction angle of the three samples changed regularly with the increase in curing days, as shown in Figure 21.

The cohesion of plain soil specimens cured for 7 d, 14 d, and 28 d was 25.05 kPa, 25.95 kPa, and 26.55 kPa, and the internal friction angle was 30.28°, 30.84°, and 31.52°, respectively. With the increase in curing time, the cohesion and internal friction angle of 7–14 d specimens were almost constant, and the cohesion and internal friction angle of 28 d specimens increased slightly. The reason may be that the moisture content of specimens in the process of curing was lower. The cohesion of MICP-reinforced soil cured for 7 d, 14 d, and 28 d was 32.7 kPa, 38.9 kPa, and 40.3 kPa, and the internal friction angle was 31.42°, 31.78°, and 32.28°, respectively. The cohesion of specimens increased with curing time. The cohesion of specimens cured for 7 to 14 d grew faster than that of 14 to 28 d, and the internal friction angle with the increase in the curing days were almost the same. Compared with plain soil, its cohesion in curing for 7 days grew by about 30%, curing for 14 days and 28 days grew by about 50%, but the internal friction angle change is small, at around 3%. The cohesion of the improved MICP-reinforced soil specimens cured for 7 d, 14 d, and 28 d was 37.65 kPa, 44.1 kPa, and 46.9 kPa, the internal friction angle was 35.44°,

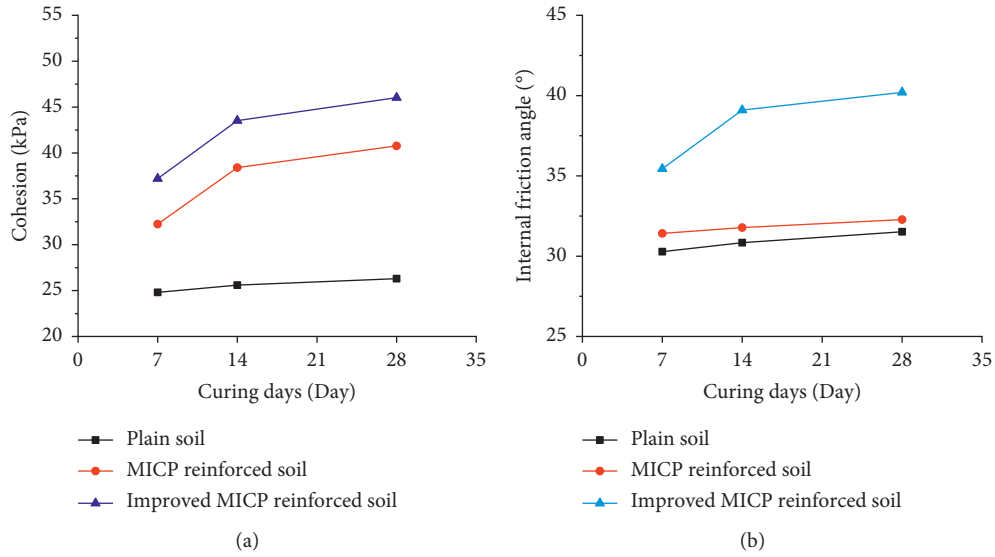

Figure 21: Variation of cohesive force and internal friction angle at different curing days. (a) Cohesion. (b) Angle of internal friction.

39.1°, and 40.2°, respectively, with the increase in the curing days. The cohesion of 7 to 14 days grew faster than that of 14 to 28 d, compared to plain soil, its cohesion in curing 7 days grew by about 50%, curing in 14 d grew by about 70%, and curing in 28 d grew by about 77%; the internal friction angle had risen about 17% in curing 7 days. Compared with the MICP-reinforced soil, its cohesion increased by about 15% at different curing days, its internal friction angle increased by about 13% at curing for 7 d, and increased by about 24% at curing for 14 d.

4.2.2. Unconfined Compressive Strength Test. Unconfined compressive strength of specimens reinforced with MICP and improved MICP was tested in strict accordance with the standard of the soil test method [33]. The axial stress and strain relationship curve of the three kinds of specimens under different curing days is shown in Figure 22.

For the same curing days, the soil reinforced with improved MICP had the maximum axial stress and the maximum corresponding axial strain, the specimens had the best resistance to failure and deformation, followed by the MICP-reinforced soil, and the plain soil had the minimum axial stress and the minimum corresponding axial strain, the specimens had the worst resistance to failure and deformation. The test results of unconfined compressive strength are summarized in Table 8.

The unconfined compressive strength of the three specimens varies regularly for different curing days, as shown in Figure 23.

With the increase in curing days, the unconfined compressive strength of soil reinforced with improved MICP for 7 to 14 d grew the fastest, with an increase rate of 34.2%. MICP-reinforced soil was the second with a growth rate of 11.2%, and that of the plain soil was the slowest with a growth rate of 5.7%. The growth rate of unconfined compressive strength of plain soil increased slightly from 14 to 28 days with an increase rate of 7.9%. The growth rate of the unconfined compressive strength of soil strengthened with MICP and modified MICP decreased to 4.0% and 7.2%, respectively. Compared with the unconfined soil, the unconfined compressive strength of the soil consolidated with MICP increased by 23%, 29.4%, and 24.6% after curing for 7, 14, and 28 d, and the unconfined compressive strength of the soil reinforced with MICP increased by 73.8%, 120.7%, and 119.1%, respectively. Compared with the MICP-reinforced soil, the unconfined compressive strength of the soil reinforced with improved MICP increased by 41.3%, 70.6%, and 75.8%, respectively, when curing for 7 d, 14 d, and 28 d.

With the increase in curing days, the axial strain to failure of the plain soil during 7 to 14 days remained unchanged. The axial strain to failure of the MICP-reinforced soil and the improved MICP-reinforced soil increased slightly, with the growth rates of 9.85% and 8.97%, respectively. During 14 to 28 d, the axial strain of plain soil, MICP-reinforced soil, and modified MICP-reinforced soil increased with growth rates of 11.86%, 8.87%, and 8.23%, respectively. During the same curing period, the deformation resistance ability of the three samples ranged from large to small from improved MICP-reinforced soil, MICP-reinforced soil, and plain soil, respectively. Compared with plain soil, the axial strain of the MICP-reinforced soil during failure increased by 11.9%, 22.9%, and 19.7% when cured for 7, 14, and 28 d, respectively. When the improved MICP was used to reinforce the soil damage, the axial strain increased by 22.9%, 33.9%, and 29.5%, respectively. Compared with the MICP-reinforced soil, the axial strain of the improved MICP-reinforced soil cured for 7 d, 14 d, and 28 d were increased by 9.85%, 8.97%, and 8.23%, respectively.

4.2.3. Analysis of Mechanical Test Results. The characteristic value of the foundation bearing capacity is decided by soil cohesion and internal friction angle. The characteristic value of the foundation bearing capacity is calculated according to formula (3), in which, f_a is the characteristic value of the

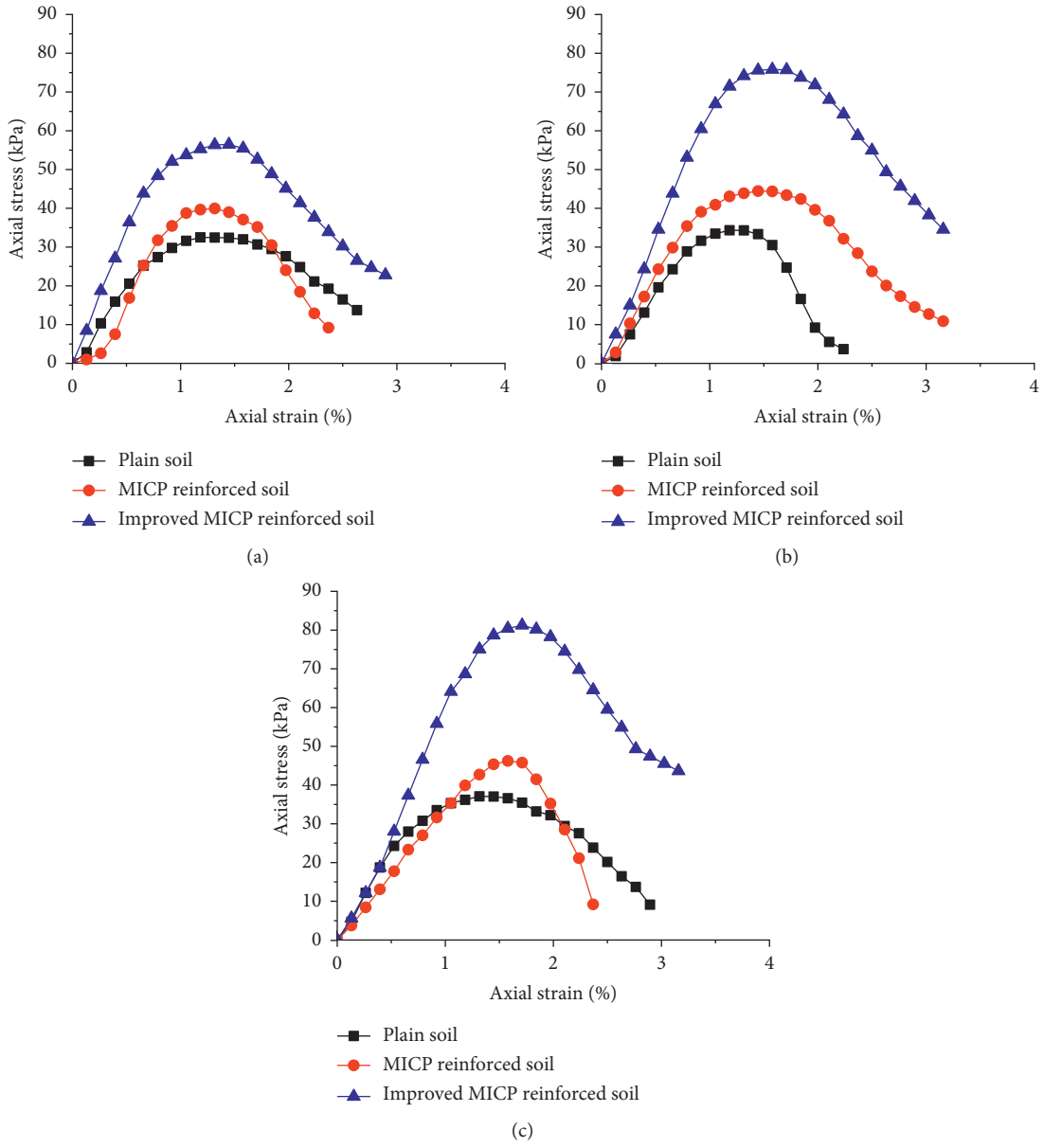

Figure 22: Relationship curve of axial stress and strain at different curing days. (a) Curing for 7 d; (b) curing for 14 d; (c) curing for 28 d.

Table 8: Unconfined compressive strength of three specimens for different curing days.

Curing days	7 d			14 d			28 d		
Sample category	Plain soil	MICP-reinforced soil	Improved MICP-reinforced soil	Plain soil	MICP-reinforced soil	Improved MICP-reinforced soil	Plain soil	MICP-reinforced soil	Improved MICP-reinforced soil
Unconfined compressive strength (kPa)	32.49	39.96	56.47	34.34	44.43	75.80	37.08	46.22	81.24
Axial strain during sample failure (%)	1.18	1.32	1.45	1.18	1.45	1.58	1.32	1.58	1.71

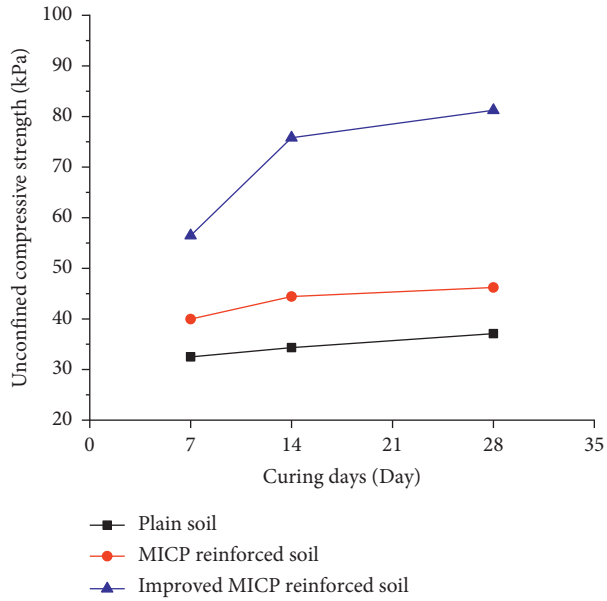

Figure 23: Change chart of unconfined compressive strength at different curing days.

foundation bearing capacity (kPa), and b is the base width. In this paper, b is taken as 6 m, c_k is the standard value of cohesion, M_b, M_c, and M_d are the bearing capacity coefficients, γ is the soil weight under the substrate, which is 18 kN/m^3, M is the weighted mean weight of soil above the base, which is 18 kN/m^3, and d is the buried depth of foundation, which is 1.5 m. According to the cohesion and internal friction angle measured in the direct shear test, the characteristic values of the bearing capacity of three soil specimens for different curing days are shown in Table 9,

$$f_a = M_b \gamma b + M_d \gamma_m d + M_c c_k. \quad (3)$$

Under ideal conditions, the characteristic value of the soil foundation bearing capacity can be calculated by formula (3). The highest characteristic value of soil foundation bearing capacity of soil improved with MICP after 28 d is its maximum compressive strength. With the increase in curing days, the characteristic value of the bearing capacity of soil foundation treated by the improved MICP method after 7 to 14 d increased the fastest, with an increase rate of 34.03%. Soil reinforced with MICP followed by an increase rate of 11.71% and plain soil was the slowest, with a growth rate of 6.03%. From 14 d to 28 d, the growth rate of the characteristic value of the bearing capacity increased slightly, with a growth rate of 6.15%. The growth rate of the characteristic value of the bearing capacity of soil reinforced by MICP and the improved MICP was reduced, with a growth rate of 5.36% and 8.21%, respectively. Compared with plain soil, the characteristic values of the bearing capacity of the ground strengthened by MICP for 7 d, 14 d, and 28 d increased by 22.87%, 29.46%, and 28.49%, respectively, which was 72.17%, 117.63%, and 121.87%, respectively, by the improved MICP. Compared with the MICP-reinforced soil cured for 7 d, 14 d, and 28 d, the characteristic values of the bearing capacity of the modified MICP-reinforced soil were 40.12%, 68.11%, and 72.67%, respectively.

5. Discussion

5.1. Effect of Glutinous Rice Slurry on Microbial Mineralization. Biomineralization refers to the process of forming inorganic minerals through the regulation of biological macromolecules. The most obvious difference from general mineralization is that the organic matrix, cells, and biological metabolites are required to participate in the process of biomineralization [47–49]. Microorganisms are widely distributed in the soil and can induce the deposition of carbonates, phosphates, sulfates, and other minerals [50–52]. In the process of mineralization, microorganisms affect the formation and regulation of the crystal form and size of carbonate particles through their metabolism and secreted metabolites [53, 54]. There are a large number of hydroxyls, carboxyls, and phosphate groups on the surface of microbial cells [55]. Under alkaline conditions, the bacteria have a negative charge, which has a strong electrostatic attraction to metal cations, which makes calcium ions free near the bacteria to form chemical bonds (as shown in formula (4)). Calcium ions combine with carbonate to form calcium carbonate. Bacteria provide mineralizing nuclear sites for calcium carbonate, which enables crystallization and mineralization of calcium carbonate near the surface of bacteria, as shown in the following formulas:

$$\text{bacteria} + Ca^{2+} \longrightarrow \text{bacteria} - Ca^{2+} \quad (4)$$

$$\text{bacteria} - Ca^{2+} + CO_3^{2-} \longrightarrow \text{bacteria} - CaCO_3 \quad (5)$$

The main components of glutinous rice slurry are starch and protein, with the protein content of 7%–10% [56, 57]. Protein can provide nitrogen and carbon required by bacteria. It was found that the protein in glutinous rice slurry could improve the activity of *bacillus pasteurella* and urease production. Urease can decompose urea to produce carbonate ion, which makes calcium ions to precipitate to

Table 9: Characteristic values of bearing capacities of specimens for different curing days.

Sample category	Curing days	Cohesion (kPa)	Angle of internal friction Φ (°)	M_b	M_d	M_c	f_a (kPa)
Plain soil	7	25.05	30.28	1.998	5.6964	8.034	462.947
	14	25.95	30.84	2.194	5.9092	8.202	490.866
	28	26.55	31.52	2.432	6.1676	8.406	521.033
MICP-reinforced soil	7	32.7	31.42	2.397	6.1296	8.376	568.832
	14	38.9	31.78	2.523	6.2664	8.484	635.462
	28	40.3	32.28	2.712	6.4704	8.6438	669.494
Improved MICP to reinforce soil	7	37.65	35.44	3.976	7.9588	9.76	797.056
	14	44.1	39.1	5.44	10.21	11.3115	1068.267
	28	46.9	40.2	5.8	10.84	11.73	1156.017

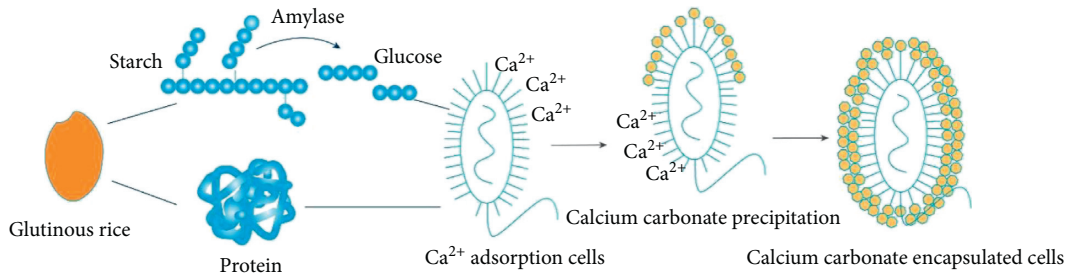

Figure 24: Schematic diagram of calcium carbonate crystallization under the action of glutinous rice slurry.

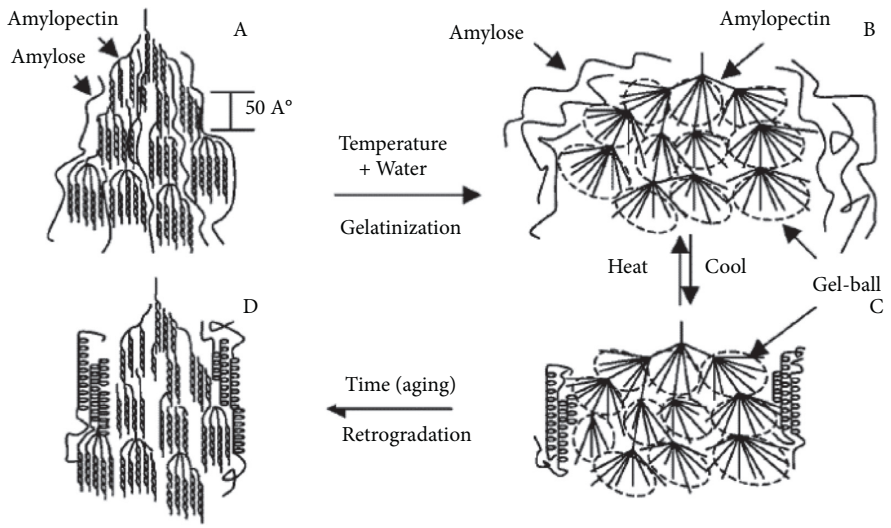

Figure 25: Molecular structure of amylopectin and amylose during gelatinization [70].

calcium carbonate. With the extension of time, glutinous rice slurry continued to play a role in promoting the formation of more calcium carbonate and prolonging the biomineralization time. The reason is that the starch content in glutinous rice slurry reaches 75%–77%. Studies have shown that some bacteria and fungi can produce amylase, and the related bacteria include *bacillus*, *aspergillus*, *streptomyces*, *trichoderma*, *penicillium*, *clostridium*, *thermomonas*, etc. [58–61]. Relevant studies have shown that *thermophilic Bacillus*, *Bacillus gelatinosa*, *Bacillus cereus*, and *Alternaria* have a certain impact on the morphology and crystal diversity of calcium carbonate [62–66]. Protein and starch play an important role in the decomposition of soil organic matter and nutrient cycling and can be used as a nutrient source for many microorganisms. The mineralized calcium carbonate crystals in glutinous rice slurry are shown in Figure 24. From the above analysis, glutinous rice slurry provides certain organic matter for the mineralization process of microorganisms, promotes the process of microbial mineralization and microbial diversity, and has an important impact on biological mineralization.

5.2. Effect of Amylopectin on Glutinous Rice Slurry. Glutinous rice slurry is rich in starch. Amylopectin is the main starch molecule, which can mineralize calcium carbonate. After the glutinous rice slurry is heated and gelatinized, the branched-chain molecules are open and form a spiral crystal structure. The adjacent branch chains form an adhesive ball structure, which can enhance the viscosity of glutinous rice slurry solution [67]. Amylopectin is a tree branch structure, which can regulate the position, size, and morphology of calcium carbonate crystals [66, 68, 69], as shown in Figure 25. The branched-chain structure can also provide coordination sites for Ca^{2+}, which makes the distribution of Ca^{2+} dendritic. Ca^{2+} reacts with the silica and alumina in the soil to form hydrated silicon (calcium aluminate) gel CSH, which makes CSH arrange in a dendritic form. The CSH dendrite network structure can cement soil particles into aggregates, which makes soil particles to connect more closely and improve the integrity of soil particles. Therefore, the mechanical properties of the silt can be improved by the amylopectin action of glutinous rice slurry.

6. Conclusion

Based on the technology of the glutinous rice mortar and the principle of biomineralization, experiments on improved silt with glutinous rice slurry, improved MICP with glutinous rice slurry, and improved silt with modified MICP were carried out, and the improvement of mechanical properties of silt by modified MICP was studied. The main conclusions are summarized as follows:

(1) The mechanical properties and microstructure of Yellow River silt with glutinous rice slurry were studied. Adding glutinous rice slurry into the silt can effectively improve the mechanical properties of soil. With the increase in the concentration of glutinous rice slurry, the strength and internal friction angle of soil samples first increase and then decrease, and the cohesion presents a linear increasing trend. The shear strength, unconfined compressive strength, and internal friction angle of 3% glutinous rice slurry are the largest.

(2) When the concentration of glutinous rice slurry is too small, amylopectin has a weak ability to control calcium carbonate crystals, and its action time is short; when the concentration of glutinous rice slurry is too high, the excess glutinous rice slurry will adhere to the surface of calcium hydroxide, which will affect the crystallization process of calcium carbonate, and then affect the improvement effect of soil.

(3) Glutinous rice slurry could improve bacterial activity and promote the formation of calcium carbonate; when the concentration of cement solution was 0.5 M and the mass ratio of cementitious liquid to bacterial liquid was 2 : 1, the optimal mass ratio of gelatinous bacteria was obtained, and the amount of $CaCO_3$ formed was the largest, and the conversion rate of Ca^{2+} was more than 80%.

(4) Based on the optimal calcium concentration (0.5 M), the optimal mass ratio of cementitious liquid to bacterial liquid (2 : 1) and improved bacterial liquid, the $CaCO_3$ production under the improved MICP technology was studied. The actual amount of $CaCO_3$ precipitated was 0.299 g, the conversion rate of Ca^{2+} was 93.44%, and the Ca^{2+} conversion rate was 12.75% higher. The results indicate that the modified MICP are able to increase the concentration of bacteria and increase the urease content in the bacterial solution and promote the production of $CaCO_3$.

(5) Through a direct shear test and unconfined compressive strength test, the mechanical properties of plain soil, MICP-reinforced soil, and modified MICP-reinforced soil are obtained. The results show that the strengthening effect of mechanical properties of the modified MICP-reinforced soil is better than the MICP-reinforced soil. MICP technology can improve the cohesion of soil, and the improvement of internal friction angle is not obvious; the improved MICP technology can not only improve the cohesion of soil, but also improve the internal friction angle, so that the mechanical properties of soil can be reinforced. With the increase in curing days, the strength of modified MICP soil increases continuously and the biomineralization time is prolonged.

Data Availability

Some or all data, models, or code that support the findings of this study are available from the corresponding author upon reasonable request.

Conflicts of Interest

There are no conflicts to declare.

Acknowledgments

This work was supported by the National Natural Science Foundation of China under project 51978634. Additional support was provided by the Department of Science and Technology of Henan Province under project 212300410012. The authors thank Kaifeng science and Technology Bureau of Henan Province for providing the bacteria for this work.

References

[1] V. C. Goreham and C. B. Lake, "Influence of water on diffusion and porosity parameters of soil-cement materials," *Canadian Geotechnical Journal*, vol. 50, no. 4, pp. 351–358, 2013.

[2] C. Shi, A. F. Jiménez, and A. Palomo, "New cements for the 21st century: the pursuit of an alternative to portland cement," *Cement and Concrete Research*, vol. 41, no. 7, pp. 750–763, 2011.

[3] M. A. M. Al-Bared, A. Marto, and N. Latifi, "Utilization of recycled tiles and tyres in stabilization of soils and production

of construction materials - a state-of-the-art review," *KSCE Journal of Civil Engineering*, vol. 22, no. 10, pp. 3860–3874, 2018.

[4] N. Zainuddin, N. Z. Mohd Yunus, M. A. M. Al-Bared, A. Marto, I. S. H. Harahap, and A. S. A. Rashid, "Measuring the engineering properties of marine clay treated with disposed granite waste," *Measurement*, vol. 131, no. 131, pp. 50–60, 2019.

[5] M. Wang, Y. Zhu, L. Cheng et al., "Review on utilization of biochar for metal-contaminated soil and sediment remediation," *Journal of Environmental Sciences*, vol. 63, no. 001, pp. 156–173, 2018.

[6] L. Cheng, R. Cord-Ruwisch, and M. A. Shahin, "Cementation of sand soil by microbially induced calcite precipitation at various degrees of saturation," *Canadian Geotechnical Journal*, vol. 50, no. 1, pp. 81–90, 2013.

[7] N. K. Dhami, M. S. Reddy, and A. Mukherjee, "Significant indicators for biomineralisation in sand of varying grain sizes," *Construction and Building Materials*, vol. 104, pp. 198–207, 2016.

[8] Y. Zhao, J. Yao, Z. Yuan, T. Wang, Y. Zhang, and F. Wang, "Bioremediation of Cd by strain GZ-22 isolated from mine soil based on biosorption and microbially induced carbonate precipitation," *Environmental ence and Pollution Research*, vol. 24, no. 1, pp. 372–380, 2020.

[9] A. A. Qabany and K. Soga, "Effect of chemical treatment used in MICP on engineering properties of cemented soils," *Géotechnique*, vol. 63, no. 4, pp. 331–339, 2013.

[10] B. M. Mortensen and J. T. Dejong, "Strength and stiffness of micp treated sand subjected to various stress paths," *Geotechnical Special Publication*, pp. 4012–4020, 2011.

[11] M. Lee, M. G. Gomez, M. E. Kortbawi, and K. Ziotopoulou, "Examining the liquefaction resistance of lightly cemented sands using microbially induced calcite precipitation (MICP)," in *Proceedings of the Geo-Congress 2020*, Minneapolis, Minnesota, February 2020.

[12] Z. Han, X. Cheng, and Q. Ma, "An experimental study on dynamic response for MICP strengthening liquefiable sands," *Earthquake Engineering and Engineering Vibration*, vol. 15, no. 4, pp. 673–679, 2016.

[13] N. J. Jiang and K. Soga, "The applicability of microbially induced calcite precipitation (MICP) for internal erosion control in gravel-sand mixtures," *Géotechnique*, vol. 67, no. 1, pp. 42–55, 2016.

[14] P. W. Glover, I. I. Zadjali, and K. A. Frew, "Permeability prediction from MICP and NMR data using an electrokinetic approach," *Geophysics*, vol. 71, no. 4, pp. F49–F60, 2006.

[15] D. Terzis, R. Bernier-Latmani, and L. Laloui, "Fabric characteristics and mechanical response of bio-improved sand to various treatment conditions," *Applied Microbiology and Biotechnology*, vol. 60, no. 1, pp. 588–593, 2015.

[16] L. I. Chengjie, W. Taoyuan, and J. I. Bin, "Study on MICP affected by different calcium sources and Ca~(2+) concentrations," *Environmental ence & Technology*, vol. 41, pp. 30–34, 2018.

[17] J. Gu, M. T. Suleiman, H. Bastola, and D. Brown, "Treatment of sand using microbial-induced carbonate precipitation (MICP) for wind erosion application," in *Proceedings of the IFCEE 2018*, Orlando, FL, USA, March 2018.

[18] P. Liu, G. H. Shao, and R. P. Huang, "Study of the interactions between S. pasteurii and indigenous bacteria and the effect of these interactions on the MICP," *Arabian Journal of Geosciences*, vol. 12, no. 23, 2019.

[19] W. Zhaoyu, N. Zhang, G. Cai, and Y. Jin, "Review of ground improvement using microbial induced carbonate precipitation (MICP)," *Marine Georesources & Geotechnology*, vol. 35, no. 8, pp. 1135–1146, 2017.

[20] F. W. Yang, B. J. Zhang, C. C. Pan, and Y. Zeng, "Traditional mortar represented by glutinous rice mortar -- one of the major inventions in ancient China," *Chinese Science*, vol. 52, pp. 1–7, 2009.

[21] K. Zhang, S. Fang, and B. Zhang, "The application history and science of traditional Chinese egg white mortar," *Chinese Science*, vol. 45, no. 8, pp. 635–642, 2015.

[22] H. Peng, Qi Zhang, and N. Li, "The effect of glutinous rice slurry on the properties of the mixed soil used for restoration of earthen sites," *Journal of Building Materials*, vol. 5, pp. 142–146, 2011.

[23] M. P. Riccardia, P. Dumiucob, C. Tomasic, and P. Ferloni, "Thermal,microscopic and X-raydiffraction studies on studies on some ancient mortars," *Thermochimica Acta*, vol. 321, no. 1, pp. 207–214, 1998.

[24] M. Fan, X. Pei, and J. Du, "Experimental study on basic physical and mechanical properties and microstructure of modified glutinous rice mortar," *Silicate bulletin*, vol. 39, no. 5, pp. 212–218, 2020.

[25] Ji Xiaojia, M. song, and M. Pang, "Experimental study on the physical and mechanical properties of glutinous rice slurry concrete," *Building technology*, vol. 44, no. 6, pp. 540–543, 2013.

[26] Q. Liu, X. Liu, and C. Pei, "The effect of glutinous rice slurry on the morphology of biomimetic calcium carbonate," *Acta intraocular lens*, vol. 43, no. 2, pp. 443–449, 2014.

[27] P. Anbu, C. H. Kang, Y. J. Shin, and J. S So, "Formations of calcium carbonate minerals by bacteria and its multiple applications," *SpringerPlus*, vol. 5, no. 1, p. 250, 2016.

[28] J. A. Ohan, S. Saneiyan, J. Lee et al., "Microbial and geochemical dynamics of an aquifer stimulated for microbial induced calcite precipitation (MICP)," *Frontiers in Microbiology*, vol. 11, p. 1327, 2020.

[29] M. A. Shahin, K. Jamieson, and L. Cheng, "Microbial-induced carbonate precipitation for coastal erosion mitigation of sandy slopes," *Géotechnique Letters*, vol. 10, no. 2, pp. 1–5, 2020.

[30] A. J. Phillips, R. Gerlach, E. Lauchnor, A. C. Mitchell, A. B. Cunningham, and L. Spangler, "Engineered applications of ureolytic biomineralization: a review," *Biofouling*, vol. 29, no. 6, pp. 715–733, 2013.

[31] X. Kong, S. Song, M. Wang, and Q. Zhao, "Experimental research of low liquid limit silt stabilized by lignin in the flooding area of yellow river," *Geotechnical & Geological Engineering*, vol. 37, no. 6, pp. 5211–5217, 2019.

[32] *Code for Design of Building Foundation (GB 50007-2011)*, China Construction Industry Press, Beijing, China, 2012.

[33] *Standard for Soil Test Method (GB/T50123-2019)*, China Planning Press, Beijing, China, 2019.

[34] B. Julia, O. Ippisch, P. Overduin, B. Hagedorn, and K. Roth, "Water, heat and solute dynamics of a mud boil, Spitsbergen," *Geomorphology*, vol. 95, no. 1-2, pp. 61–73, 2008.

[35] H. U. Zaiqiang, Y. U. Miao, L. I. Hongru, and L. Jin, "Experimental study on characteristics of artificial soil ruins," *Chinese Journal of Rock Mechanics and Engineering*, vol. 35, no. 9, 2016.

[36] C. Kai, W. Dong-Hua, C. Wen-Wu, and W. Ren, "Comparative study of anchorage performance of three types of bolts fully grouted by modified glutinous rice mortar," *Rock and Soil Mechanics*, vol. 39, no. 2, pp. 498–506, 2018.

[37] C. Wen-Wu, Y. Guang, and C. Kai, "Field penetration test to strengthen the scaling off of earthen sites," *Journal of Lanzhou University*, vol. 53, no. 3, 2017.

[38] D. Kong, J. Chen, R. Wan, and H. Liu, "Study on restoration materials for historical silty earthen sites based on lime and starch ether," *Advances in Materials Science and Engineering*, vol. 2020, no. 6, 16 pages, Article ID 2850780, 2020.

[39] J. A. P. Pollacco, J. Fernández-Gálvez, and S. Carrick, "Improved prediction of water retention curves for fine texture soils using an intergranular mixing particle size distribution model," *Journal of Hydrology*, vol. 584, Article ID 124597, 2020.

[40] T. Wei, W. Fan, and W. Yuan, "Three-dimensional pore network characterization of loess and paleosol stratigraphy from South Jingyang Plateau, China," *Environmental Geology*, vol. 78, no. 11, pp. 333.1–333.15, 2019.

[41] A. I. Omoregie, L. H. Ngu, D. E. L. Ong, and P. Nissom, "Low-cost cultivation of Sporosarcina pasteurii strain in food-grade yeast extract medium for microbially induced carbonate precipitation (MICP) application," *Biocatalysis and Agricultural Biotechnology*, vol. 17, no. 11, 2019.

[42] J. Zhang, W. Liu, D. Guan, and Y. Zhou, "Influence of different bacterial grouting strategies on MICP one-phase injection method," *Journal of Hohai University*, vol. 48, no. 3, pp. 222–230, 2020.

[43] S. Atashgahi, A. Tabarsa, A. Shahryari, and H. Seyedeh, "Effect of carbonate precipitating bacteria on strength and hydraulic characteristics of loess soil," *Bulletin of Engineering Geology and the Environment*, vol. 79, no. 4, 2020.

[44] M. A. Imran, S. Gowthaman, K. Nakashima, and S Kawasaki, "The influence of the addition of plant-based natural fibers (Jute) on biocemented sand using MICP method," *Materials*, vol. 13, no. 18, 2020.

[45] S. Z. Zhang, J. Li, and J. Li, "Determination of calcium content in ferrosilicon nitride by EDTA titration," *Ferroalloy*, vol. 48, no. 10, pp. 45–48, 2017.

[46] S. Baotang, S. Jingyu, and B. Nick, "An approximate nonlinear modified Mohr-Coulomb shear strength criterion with critical state for intact rocks," *Journal of Rock Mechanics and Geotechnical Engineering*, vol. 10, no. 4, pp. 37–44, 2018.

[47] T. Huang, M. X. Liu, and F. Q. Dong, "Comparative study on calcium strontium biomineralization induced by different microorganisms," *Acta Geologica Sinica*, vol. 21, no. 4, pp. 584–593, 2015.

[48] Y. Fang, J. W. Liu, and Q. B. Gu, "Application of biomineralization in environmental protection," *Silicate bulletin*, vol. 36, no. 4, pp. 1209–1233, 2017.

[49] H. Li, Q. Z. Yao, and G. T. Zhou, "Biomineralization and biomineralization in nano scale:a mesomorphic perspective," *Earth Science*, vol. 43, no. 5, pp. 1425–1438, 2018.

[50] P. H. Lin and W. J. Ju, "Bacterial induced calcium carbonate mineralization and its application prospect," *Journal of Building Materials*, vol. 12, no. 4, pp. 482–486, 2009.

[51] Q. M. Shen, Z. Q. Huang, and G. S. Zhang, "Biomimetic synthesis of aragonite spherical superstructures at room temperature and pressure," *Journal of Materials Science and Engineering*, vol. 3, pp. 453–457, 2012.

[52] Y.-Y. Wang, Q.-Z. Yao, H. Li, G.-T. Zhou, and Y.-M. Sheng, "Formation of vaterite mesocrystals in biomineral-like structures and implication for biomineralization," *Crystal Growth & Design*, vol. 15, no. 4, pp. 1714–1725, 2015.

[53] B. Xiao, B. Lian, and W. Shao, "Do bacterial secreted proteins play a role in the weathering of potassium-bearing rock powder?" *Geomicrobiology Journal*, vol. 29, no. 6, pp. 497–505, 2012.

[54] M. D. Li, L. Lin, and Z. D. Zhang, "Progress, prospect and engineering application technology design of microbial mineralized calcium carbonate soil improvement," *Acta civil engineering*, vol. 49, no. 10, pp. 80–87, 2016.

[55] J. Tian, "Technology and application of microbial induced calcium carbonate crystallization to strengthen subgrade soil," *Highway and automobile transportation*, vol. 4, pp. 112–114+119, 2017.

[56] T. Yang, Y. Jiad, and H. R. Ma, "Effects of chemical components of glutinous rice on fermentation and quality of rice wine," *Food Science and Technology*, vol. 40, no. 5, pp. 119–123, 2015.

[57] Y. Zhou, H. F. Qian, and H. Zhang, "Study on the relationship between chemical components of glutinous rice and starch aging of rice cake," *Food industry science and technology*, vol. 16, pp. 136–139, 2013.

[58] T. Nakada and M. Kubota, "Purfication and haraterization of two forms of maloctraos-forming amylase from Pseudomonas shterl," *Agricultural & Biological Chemistry*, vol. 54, no. 53, pp. 737–743, 1990.

[59] R. Yamaquchi, H. Tokunaga, M. Ishibashi, T. Arakawa, and M. Tokunaga, "Salt-dependent themo teversible a amylase: cloning and haracteriation of halophilie a-amylase from moderately halophilic bacterium,Kocuria varians," *Applied Microbiology and Biotechnology*, vol. 89, no. 3, pp. 673–684, 2011.

[60] D. Mehta and T. Satyanarayana, "Biochemical and molecular characterization of recombinant acidic and thermostable raw-starch hydrolysing α-amylase from an extreme thermophile Geobacillus thermoleovorans," *Journal of Molecular Catalysis B: Enzymatic*, vol. 85-86, no. 4, pp. 229–238, 2013.

[61] T. Kancko, T. Ohno, and N. Ohisa, "Purification and chraterization of a thermostable raw starch digesting amylase from Sireplomyces sp. Isolated in a milling factory]," *Bioscience Biotechnology & Biochemistry*, vol. 69, no. 6, pp. 1073–1081, 2005.

[62] J. Tourney, B. T. Ngwenya, J. W. Fred Mosselmans, and M. Magennis, "Physical and chemical effects of extracellular polymers (EPS) on Zn adsorption to Bacillus licheniformis S-86," *Journal of Colloid and Interface Science*, vol. 337, no. 2, pp. 381–389, 2009.

[63] S. Stocks-Fischer, J. K. Galinat, and S. S. Bang, "Microbiological precipitation of CaCO3," *Soil Biology and Biochemistry*, vol. 31, no. 11, pp. 1563–1571, 1999.

[64] L. Wang, Y. F. Chen, and L. Yang, "Isolation and identification of amylase producing Bacillus," *Food Research and Development*, vol. 38, no. 6, pp. 175–177, 2017.

[65] H. Yang, J. K. Yang, and Y. J. Yan, "Isolation, identification and characterization of α-amylase producing strain," *Biotechnology*, vol. 17, no. 2, pp. 34–37, 2007.

[66] X. J. Liu, J. L. Li, L. Xiang, and R. Zhang, "The role of matrix proteins in the control of nacreous layer deposition during pearl formation," *Proceedings of the Royal Society B*, vol. 279, no. 7, pp. 1000–1007, 2012.

[67] W. W. Chen, Q. Y. Zhang, and H. W. Liu, "Influence of glutinous rice slurry temperature on strengthening site soil with glutinous rice mortar," *Journal of rock mechanics and engineering*, vol. 36, no. S2, pp. 4244–4250, 2017.

[68] Y. Ma, L. Qiao, and Q. Feng, "In-vitro study on calcium carbonate crystal growth mediated by organic matrix extracted from fresh water pearls," *Materials Science and Engineering: C*, vol. 32, no. 7, pp. 1963–1970, 2012.

[69] T. Yang, X. Ma, B. J. Zhang, and H. Zhang, "Investigations into the function of sticky rice on the microstructures of

hydrated lime putties," *Construction and Building Materials*, vol. 102, no. 1, pp. 1051–1053, 2016.

[70] L. Yu and G. Christie, "Microstructure and mechanical properties of orientated thermoplastic starches," *Journal of Materials Science*, vol. 40, no. 1, pp. 111–116, 2005.